



Article

On the Blueprint of the Long Primary Afferent Axons and the Dichotomous Axon Trajectory of Clarke's Nucleus. A Morphological Tracing Study on the Effect of Hypoxia during Development

Frits C. de Beer ^{1,*} and Harry W. Steinbusch ² ¹ Oleanderlaan 15, 8024 XC Zwolle, The Netherlands² Department of Neuroscience, Maastricht University, 6211 LK Maastricht, The Netherlands; h.steinbusch@maastrichtuniversity.nl

* Correspondence: fcdebeer@gmail.com

Abstract: The primary afferent system in the rat's spinal cord starts to develop in the third last week of gestation. First, the pseudounipolar DRG neurons extend their centripetal long primary axons, targeting rostral supra-segmental nuclei in the spinal cord. Meanwhile, the subsequent innervation of the juxta- and intra-segmental spinal levels enables the three subdivisions to commence integrating a complex network with the body periphery. This process may continue to refine and adapt the system life-long. The experimental data elucidated the steps involved in developing the cytoarchitecture by separating the axons of the long and intermediate subdivisions from the short subdivision. Here, we present a blueprint of the features of the long primary afferent axons developing in sequential waves. The pioneering long afferent axons targeted the dorsal gracile nuclei at spring tide and Clarke's nuclei at neap tide in ventrally bent trajectories. The paradigm's myelotomy blocked these pioneering fibers from stepping down the developmental cascade, rendering an unknown phenotype. This reflected a hypothetical transition hub stationed on the assembly line, delineating a critical period. The paradigm also affected the neuropil's ripening independently from the long primary afferent system. The data disclosed that fetal hyposaturation yielded an in vivo genomic engineering capability. Fetal tissue was susceptible to hyposaturation, showing remarkable versatility early in fetal life. The translational impact may favor research into the elusive etiology of clinical syndromes concerning the afferent system relating to fetal hyposaturation.

Keywords: Clarke's nucleus; development; DRG neurons; fetal hyposaturation; HRP; injury; spinal cord



Citation: de Beer, F.C.; Steinbusch, H.W. On the Blueprint of the Long Primary Afferent Axons and the Dichotomous Axon Trajectory of Clarke's Nucleus. A Morphological Tracing Study on the Effect of Hypoxia during Development. *Anatomia* **2023**, *2*, 414–449. <https://doi.org/10.3390/anatomia2040032>

Academic Editor: Francesco Fornai

Received: 4 July 2023

Revised: 8 November 2023

Accepted: 15 November 2023

Published: 6 December 2023



Copyright: © 2023 by the authors. Licensee MDPI, Basel, Switzerland. This article is an open access article distributed under the terms and conditions of the Creative Commons Attribution (CC BY) license (<https://creativecommons.org/licenses/by/4.0/>).

1. Introduction

The long primary afferent axons in the spinal cord convey body input directly in a centripetal flow as far rostrally as the medulla. This hardware is a multilevel architecture built in rats in the third week of gestation. The system begins with integration and increased functionality as soon as possible and continues to refine and adapt beyond birth and during its life [1]. The complex building of this system is a staged process creating three subdivisions [2]. The long-ranging fibers develop upstream of the assembly line first before the short subdivision's anlage at the level of the DREZ in rats and mice [3–10]. Our study of the pioneering primary afferents of the long and intermediate subdivisions depended on experimentation in very immature embryos, jeopardizing their survival. A genetic tracing study in mutant mice embryos documented the functional organization of the afferent fiber tract mapping [11]. Our initial investigations focused on the manipulation of fetal rats [12,13]. Based on that work, immaturity relating to anticipated healing after lesions of the immature spinal cord redirected our paradigm, endeavoring upon the cascade's upstream route. By then, the view that the incapacity to recover from a spinal cord lesion

correlated with maturity had gained consensus. Our first unpublished results demonstrated that a spinal cord lesion lacked neither any feature of repair from the immature primary afferent system nor a sign of true spinal cord healing. Due to our investigation's basic plan for the DC development, we adhered to the paramount longitudinal sectioning of the spinal cord. Misfortune's deception had invigorated our endeavors on a long and winding road to the upstream territory of spinal cord development.

In a recent paper, we addressed the genome engineering potentiality of the paradigm, which manifested serendipitously [14]. At last, that opened the door to tackle many dialectics in the data archived. The unknown phenotypes of the long primary afferent axons being exposed, distinguishing affected developmental features from identified normal ones, had to be an effect of hyposaturation. Fetal hypoxia was speculated to retard development. The confounding features were associated with dissociated ripening of the neuropil. Here, we present this retrograde study into the primary afferent system's development, uncovering mutuality between the long and intermediate subdivisions. We propose a blueprint for the system's assemblage in fetal rats, delineating its critical period. Finally, we consider the future impact of the paradigm for translational research.

2. Material and Methods

The work presented in this paper pre-dates the European legislation on animal welfare and institutional ethics board approval. An optimal housing facility and husbandry reflected the highest ethical standards applicable at that time. The in-house bred pregnant rats or those dispatched from commercially available Wistar Albino-Glaco strains served the experiments through the years. The pre-, intra-, and post-surgical animal care necessitated continuous optimization, documented with the lowest possible mortality rates among dams and neonates [12–14]. The inhalation anesthesia offered great improvement in animal handling. It greatly reduced the recuperation times and may as well have impacted the rats' well-being and long-term survival. The focus on mortality evoked the impetus to keep the figures down. Misfortune, though, was never far away and counteracted with perseverance. For an extensive description of the techniques involved, we may refer the reader to the three previous papers, which provide detailed information about the paradigm [12–14]. In short, the microsurgical dorsal myelotomy at random cervical and thoracic levels aimed to disrupt the fetal rat's primary afferent system's development, hampering the assembly line's process. The dam's conception day was scheduled fifteen to seventeen days in advance of M_0 , covering the long primary afferent system development in E15–E17 fetuses. The spontaneously breathing dam recovered within one or two minutes of quitting fluothane inhalation after the procedure, which took approximately half an hour. The success of dorsal myelotomies gradually reached almost 100%, complying with the need for suitable tracing candidates, 75% of which had been selected from whole litters, as shown in Table 1. High figures might value the standardization of complex technical procedures [15]. Applying the Horse Radish Peroxidase (HRP) to the proximal stump of the left sciatic nerve was straightforward. The spinal cords had been sectioned sagittally for processing, with a few exceptions of horizontal sections. According to Mesulam, enzyme histochemistry involved TMB [16]. The process of evaluating the lesion site was far less efficient. About one out of six of the cohort of 248 operated fetuses exhibited proper labeling after enzyme histochemistry [14]. Some more figures linked to different steps in the process chain suffered greatly from mishaps and technical flaws in our series.

For that reason, the data covered forty-five cases [14]. The lesion sites aimed at thoracic levels appeared accordingly, with a few exceptions from cervical levels. Labels present in the gracile nuclei disqualified a few cases due to a DC-transection (Tx), which was far too low at the DREZ proper. A caudad lumbar level might have yielded unharmed primary afferents bypassing the lesion in the DREZ. This paper recovered the data from eleven cases (Figures 6–16 and 19), with successful tracer features listed in Table 1, which also entailed another thirty-four cases with superfluous or incomplete features. Figure 19 encompasses five cases exhibiting the neuropil's label boosted in the primordial state.

Bell ringers from fully processed experiments.

Table 1. (a) tallies 27 cases processed successfully after HRP tracing. Column 1 entails fully processed experiments, denoted by a threefold letter-and-number combination, showing the serial number first and the follow-up period third. The Tx day (M_0) relates to the conception day noted in the middle, specified by the hour in a few. Column 2 colors the success ratios in red (count of Tx: fetus count = the litter size). Fewer than expected dead neonates resulted from stillborn and cannibalism. Column 3 lists eleven cases displayed in Figures 6–16 and 19. Column 4 lists thirteen cases with uncovered features of upstream development. Cases with dissociated neuropil are listed in column 5. (b) tallies 18 cases eligible for tracing procedures offering minor data due to technical flaws and mishaps. We skipped five cases with a DREZ lesion. the left sciatic nerve had been transected at the caudal rim of the m.gluteus on p2 as an intended preconditioning lesion. Assessment of hypoxic preconditioning in the CNS dates from ten years ago (see Sections 3.2.4 and 4.2.4).

1	2	3	4	5	1	2	3	4	5
Case	litter-ratio (Tx:n = p0)	Figures	upstream features	dissociated neuropil	Case	litter-ratio (Tx:n = p0)	Figures	upstream features	dissociated neuropil
C39.E18.E20	N/A				C44.Sx.p4	N/A			
D20.D17.E18	N/A				D14.D5.E21	N/A			
D15.E17.E20	N/A				P1.p48	(2:15 = 14 + 1 †)			
N45.E17.p8	(1:4 = 4)				P20.p600	(2:9 = 8)			
N46.E18.p10	(2:15 = 15)				R9.S6.p44	(4:11 = 11)			
T8.E17.p180	(2:15 = 15)				R9.S4.p44	(4:11 = 11)			
T16.E17.p40	(2:15 = 13)				T9.2.p225	(3:15 = 12)			
T20.E17.p700	(1:9 = 7)	Figure 19f	X	X	T12.p7	(2:15 = 15)			
T23.E16.p360	(1:6 = 6)				T13.p7	(2:14 = 12)	Figure 19a,b	X	X ¹
T45.E16.p7	(1:4 = 4)	Figure 6			T15.p305	(3:16 = 14)	Figure 19e	X	X
T46.E16.p3	(1:13 = 12 + 1 †)	Figure 14	X	X	T34.p100	(1:8 = 8)			
T47.E16.p4	(1:2 = 2)	Figure 8	X		T42.p240	(1:9 = 9)			
T60.E16+12h.p135	(1:10 = 10)				T62.p17	(2:11 = 11)			
T77.E16.p35	(1:12 = 12)	Figure 12	X		T65.p48	(1:10 = 10)	Figure 19c	X	X
T78.E16+2h.p40	(1:8 = 7)	Figure 15	X	X	T68.p370	(1:11 = 11)			
V2.E16-1h.p240	(2:14 = 13)	Figure 11	X		V1.p600	(1:10 = 9)			
V3.E16-1h.p195	(1:13 = 12 + 1 †)	Figure 13	X		W6.p32	(2:14 = 14)			
V31.E16-3h.p145	(1:13 = 13)	Figures 10 and 19d	X	X	W17.p64	(1:14 = 14)			
V38.E16-3h.p210	(1:15 = 15)								
V51.E16-4h.p2	(1:9 = 9)		X						
V63.E16-2h.p1.5	(1:11 = 11)								
V67.E16+7h.p9	(1:7 = 7)	Figure 16	X	X					
V72.E16+8h.p1.5	(1:14 = 14)		X						
W2.E16-8h.p8	(2:10 = 10)	Figure 7	X						
W2.E16-5h.p42	(2:10 = 10)								
W14.E16-8h.p14	(2:15 = 15)								
W20.E16-9h.p6	(2:11 = 9)	Figure 9	X						

†: one stillborn present in the litter; X¹: a preconditioning lesion by transection of the left sciatic nerve in the neonate at p2.

Commentaries

The HRP application to the proximal stump of the sciatic nerve was a fast and easy procedure in neonates and adult rats of this series. To its great advantage, the HRP application was feasible in the fetus, favoring it as the tracer of our choice. The anterograde transport of HRP outran any other tracer by its speed of 10 cm/day [17]. These properties made it extremely valuable despite many drawbacks. Standardization helped tackle related problems. The mounting skills never prompted us to avoid applying this ‘arch mother’ of neuroanatomical transport tracers [17]. In hindsight, this retrograde study showed a few shortcomings. The number of axons traced was unknown. The paradigm’s exerted effect on axon numbers or time specification was undetermined. The extent of fetal hyposaturation, of which the length and severity of hypoxia might have been decisive, was not an issue. However, inhalation anesthesia intentionally improved the survival rates of fetuses [14]. Despite these flaws, the data made intriguing observations of previously inaccessible territory possible.

Glossary

a-FS	abrupt front stop	WM-facing rostral bundle of cut high-tide primary afferents blocked at the TH.1 stage and abutting the lesion site caudally
CP	critical period	upstream time slot(s) for each (and all) pioneering long primary afferent axon(s)
CG	central gray	or referred to as immature neuropil
	colls	TH.2-staged collaterals = collateral sprouting following TH.2 transit and illustrating unrestrained development displayed in the neuropil or dystopically within the DC-WM
DRG	dorsal root ganglion	involving the lumbar segments L4, L5, and L6 (at the left side)
DC	dorsal column	or the neuropil covering dorsal WM
DH	dorsal horn	
DREZ	dorsal root entry zone	
E16-8h	15 th day of gestation	M ₀ is scheduled 15 days + 16 h after mating, restricted to 1 h
E16		day of conception without surveillance of mating time
f-ES	fast elongation stop	hypothetical configuration figuring the swift downregulation of elongating TH.0-staged pioneering axons at the medulla
FOV	field of view	a microscopic segment of a tissue section
	fiber resorting	central branches networking into functional circuitries, presumably in concert with peripheral branches
	fringe	the CG, adjacent to the DC-WM
	high tide	in the rostral DC, pioneering axons target the gracile nuclei in high-tide waves at spring tide
i-FS	individual front stop	a low-tide axon blocked at the TH.1 stage, featuring its fiber ending distanced from the lesion site
	low tide	in the lower thoracic DC, pioneering axons target Clarke's nucleus in low-tide waves at neap tide
M ₀		moment of Tx referenced to the hour (or day) of conception
	neap tide	a case identifier in combination with survival time
	primordial state	see low tide
	reciprocity	due to temporospatial dissociation (see the legend of Figure 18)
s-ES	slow Elongation Switch	low- and high-tide axons share a common trajectory in the DC-WM
	spring tide	the transitioning of a TH.1 axon before creating collateral sproutings (colls)
TMB		see high tide
		Tetramethylbenzidine
THs	transition hubs	TH.0, TH.1, TH.2, and TH.3 situate hypothetically on the developmental cascade, figuring unknown phenotypes which disclose TH.1, TH.2, and TH.3 stage features after Tx (see Section 3.1.1)
TH.0	staged axon	pioneering primary afferent axon in a high- or low-tide wave
TH.1	staged axons	a rostral Tx created an axon bundle at spring tide featuring the a-FS, or multilevel i-FSs in a caudal thoracic Tx at neap tide
Tx	dorsal myelotomy	the microsurgical procedure
VREZ	ventral root exit zone	
WP	Waiting Period	time window beyond the CP followed by the fiber resorting process
WM	white matter in DC	WM-DC, or DC-WM

Figure legends

*/**	asterisk/s	a single asterisk indicates a TH.1-staged i-FS; a tandem asterisk indicates colls
---	interrupted	the red line indicates a remnant of low-tide axons delineating the hypertrophic Clarke's nucleus in the ripened neuropil
	uninterrupted	the red line encompasses the inaccessible neuropil
	basion	the caudal rim of the clivus in front of the medulla (Figure 14e)
	obex	at the level of the medullary aperture into the central canal
CC	central canal	of the spinal cord
	CG-in-DC	dystopic CG in the midline, a remnant of a fetal myelotomy or its anlage
C.nu	Clarke's nucleus	
g.nu	gracile nucleus	
4th V	fourth ventricle	
	L Th C	Lumbar Thoracic Cervical segment of the spinal cord
	c <== ==> r	caudal <== ==> rostral direction of the spinal cord
	d <== ==> v	dorsal <== ==> ventral in a sagittal section of the spinal cord
	~~ X ~~	~~ at about the -estimated- spinal level of X ~~
l.s.	lesion site	
L/R	left side/right side	of the spinal cord in a horizontal section
N	fix pinhole	an artifact from tissue processing; a number identifies the spinal cord's level derived from the gelatine block's count

3. Results

First, a detailed preview in Section 3.1 might help explain the intricate temporospatial assemblage of the long primary afferent system. We describe the developmental characteristics disclosed by the affected afferent axons. The analysis revealed the Tx's impact on the upstream developmental steps. An outline of the assembly line starts with the long primary axon features linked to their upstream stages. The temporospatial development follows and exhibits the dynamic interplay between the two long subdivisions. Next, the developing Clarke's nucleus, coinciding with the upstream neuropil's ripening, highlights the paradigm's two-edged impact. Those features are confounding.

To present the results of this retrograde investigation, we have ordered the cases downward according to the developmental cascade, following the primary afferent system's blueprint. To appreciate a shift down the cascade, the first two sets of slides from neonates and adult experiments help create the picture of the characteristic configurations rendered by the Txs. The third set shows the effects at utmost upstream M_0 s, i.e., of primordial interference.

The results in Section 3.1 show the afferent axon basics. Section 3.2 encompasses the Tx features. Random upstream M_0 s reflect a tight link with the critical period's time window.

3.1. The Assembly Line

3.1.1. Identification of Axon Types at the Transition Hubs

Hubs in regulatory networks might refer to transition factors (TFs). We assigned the transition hubs (THs) to an intricate web of successive TFs within the unknown intrinsic developmental plan accomplished by the DRG neurons. We conceptualized a potential assembly line stationed with four hypothetical THs: TH.0, TH.1, TH.2, and TH.3. "Vis vitalis" initiated the development process, governed by an intrinsic developmental plan. The TH.0-staged pioneering long primary afferent axons elongated from lumbar DRGs to the rostral medulla. Those upstream fibers instantly reduced their elongation speed, arriving at the medulla. This swift transit altered a hypothetical TH.0 proteomic profile into a consecutive TH.1. We named this phenomenon the fast elongation stop (f-ES). Further down the assembly line, development entailed the equation of the elongation speed according to the spinal cord growth. This step in the cascade might take time. We called it the slow elongation switch (s-ES). Next, the axons started developing fiber collaterals (colls) down at TH.2. This extended process implied subsequent fiber resorting and functional adaptation of the afferent system, which might result in a distinguishable third TH.3 [9]. These hidden transitory stages became perceptible after Txs, uncovering the development process.

For clarity, the developmental stages are colored according to the hypothetical transitory THs, green, yellow, light brown, and dark brown in the high-tide waves (Figure 1a). In low-tide waves, yellow turns into ocher (Figure 1b). The high- and low-tide waves harbored the axons pioneering to gracile and Clarke's nuclei, addressed in Section 3.1.2. Identifying the axon's features by sorting the HRP label configurations was pivotal for the conceptualization of a blueprint of the TH-stationed assembly line. This enabled the creation of a slow-motion picture film of the sorted stills acquired in random experiments. Notably, the CP was responsible for countless configurations of axon features, reflecting multistage axons. Figure 2b(1–5) depict five particular schematic examples in a subsequent order down the assembly line.

Four uncovered phenotypes in the DRG neuron transitioning from axon elongation to collateral fiber formation in (a) the long and (b) the intermediate primary afferent system.

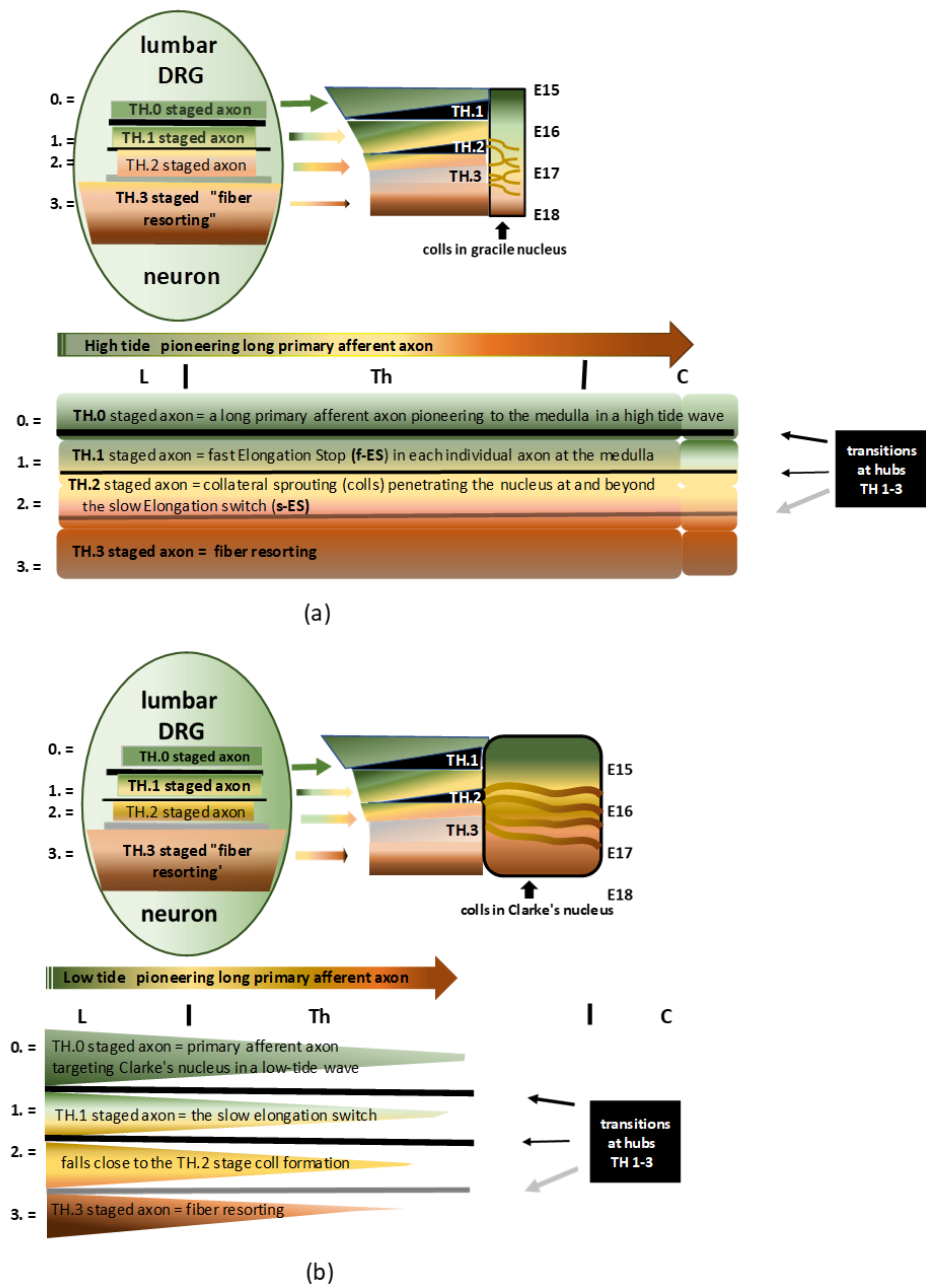


Figure 1. (a) Infographic of the DRG neuron’s development governing the central branch’s long primary afferent pioneering axon and maturation in a high-tide wave to the gracile nucleus. The four consecutive stages on the assembly line are colored green, yellow, light brown, and dark brown, denoted by 0, 1, 2, and 3, respectively. The pioneering axon is colored green; beyond the f-ES, the axon is colored yellow; the s-ES turns the axon light brown and entails the TH.2 stage of colls; next, the axon is colored darker brown, figuring the fiber resorting process. The modesty of the black and grey bars masks the complexity of the hypothetical in-between transition hub (TH) network. The stations on the assembly line build the developmental cascade of the long primary afferent system. See the text for descriptive details. (b) Infographic of the DRG neuron’s development governing the central branch’s long primary afferent pioneering axon and maturation in a low-tide wave to Clarke’s nucleus. The four consecutive stages on the assembly line are colored green, ochre, light brown, and dark brown, denoted by 0, 1, 2, and 3, respectively. The color ochre indicates the axon terminates less far rostral. The slow elongation switch might fall close to the initiation of collateral formation.

3.1.2. The Abrupt Front Stop, the Individual Front Stops, and the Colls at the Cascade

Surprisingly, the microsurgical intervention caused features that gained visibility directly on the development of the primary long axons of two subdivisions. Since the nineties, research has focused on development, shifting away from the regeneration issue [18]. Understanding the above outline was a prerequisite for analyzing the data. The antegrade transport for growth cone formation is well studied [19]. Assuming that the first detectable axons belonged to the rostral rootlets of the traced sciatic nerve, we postulated a spring tide of pioneering afferents in the most energetic high-tide waves originating from lumbar DRG neurons. Afterward, axons in less dynamic low-tide waves might delineate Clarke’s nucleus at the neap tide. Transected axons recuperated. Next, they transported the label to the fiber tips. The rostral Tx of high-tide axons offered that key feature. When the fiber tips had just reached the medulla and stayed put after the f-ES, a Tx of their TH.1-staged axons might cause the abrupt Front Stop (a-FS). This rostral a-FS delineated the caudal margin of the lesion site, exemplified by the experiments in the two neonates (see Figures 7 and 9). The low-tide axons terminated caudally from the lesion site in downstream waves. Exemplarily, caudal Tx caused the i-FSs in adult cases. This key feature complied with the less dynamic neap tide. We conceptualized the data by designing a graphical flowchart depicting the primary afferent system’s hypothetical THs stationed on the assembly line (Figure 2a). The cascade’s inclination (at 3A) reflects retardation due to the nuclear and axonal mechanisms involved. At 3B, the paradigm’s impact of hypoxia on the assembly line causes increased delay, depicted by altered inclination. This delay might be maximized in barbiturate anesthetized rats, shaded gray at 3C [20,21]. In the natural design of three subdivisions, the last short subdivision might subservise the fiber resorting process by relaying the inputs of all the integrating afferent circuitries [18,22].

The blueprint of the long primary afferent system.

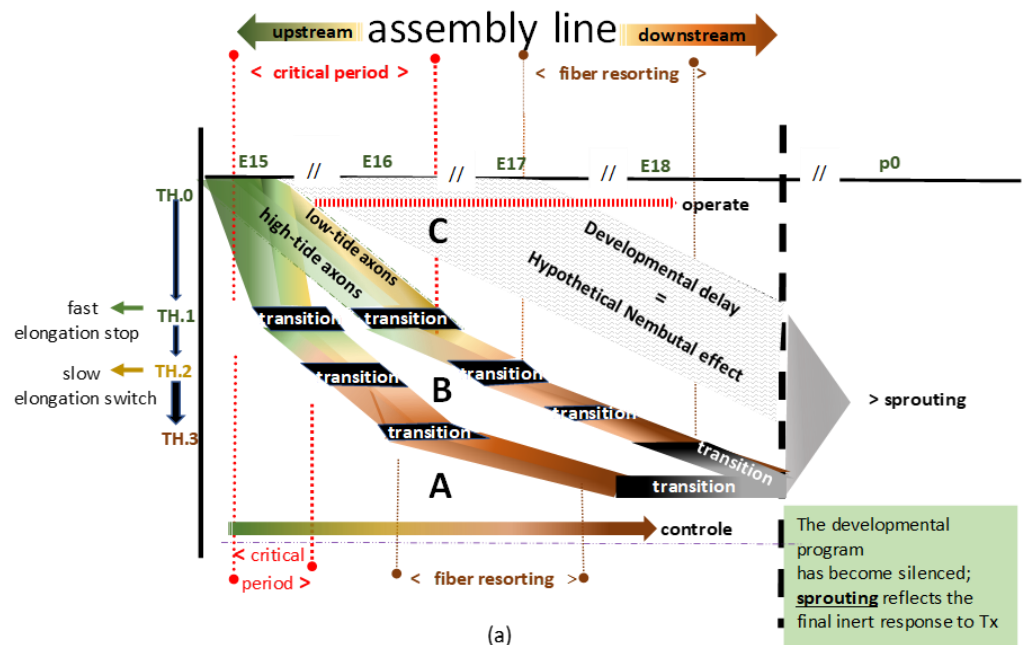


Figure 2. Cont.

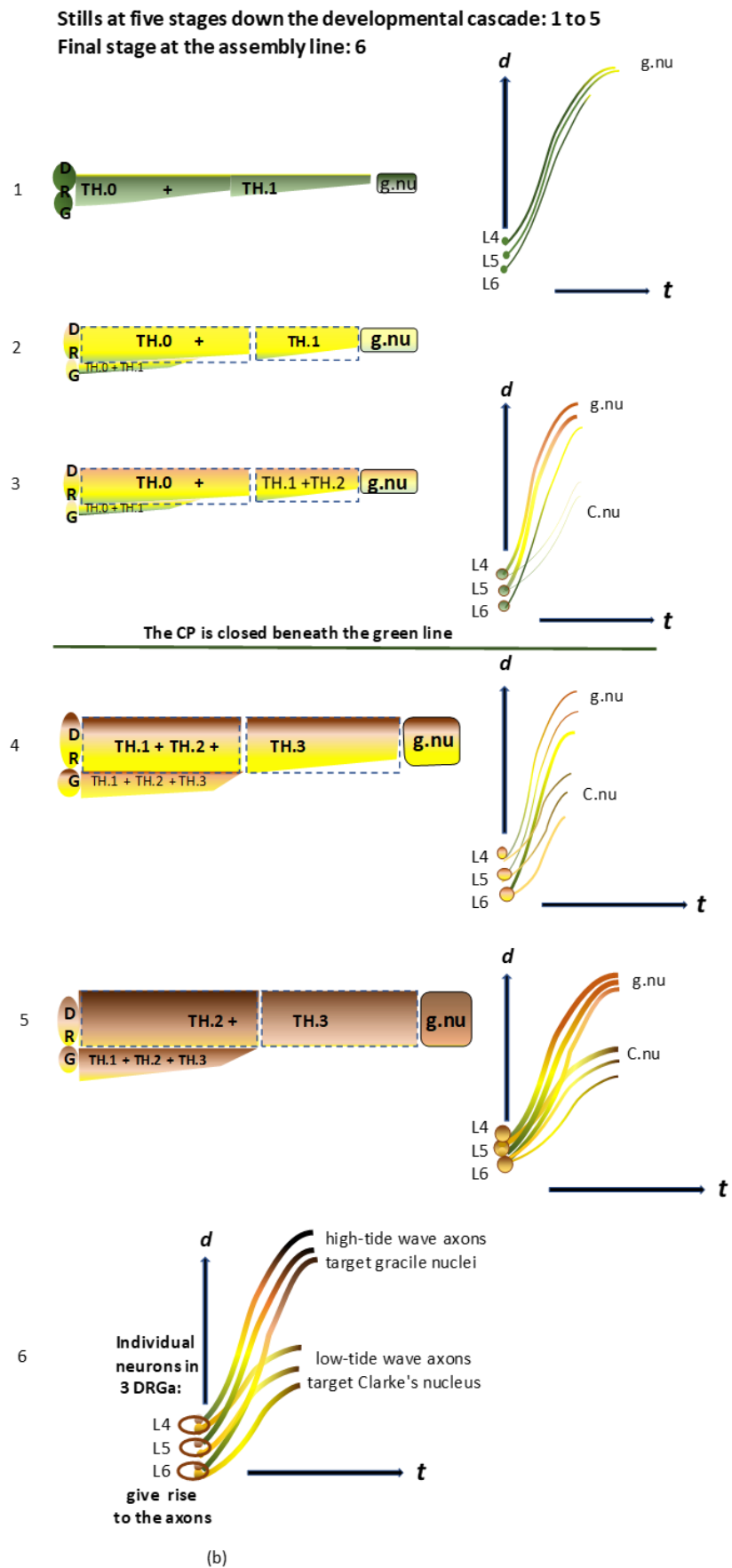


Figure 2. (a) Two flowcharts (A and B) depict a blueprint of the TH-stationed assembly lines, imaginable

for the long primary afferent system at high- and low-tide development. The black boxes represent the conceptual assembly line's transition hubs (THs). For convenience's sake, 'transition' denotes the intricate transitioning into the subsequent unknown phenotype at TH.1, TH.2, and TH.3. The downstream grey box represents the final stage. The inclination of developmental speed might vary, as demonstrated by the two hypothetical examples, A and B, and the dashed area C. The variation might depend on the extent of hyposaturation determined by hypoxia, of which the depth and the length of time are unknown parameters. A shows development under natural conditions and B shows delay due to the paradigm. In C, the gray area delineates a tentative interpretation of the excessive delay due to barbiturate anesthesia. The high- and low-tide pioneering axons are green. The colors turn brown and dark brown when all TH.2- and TH.3-staged axons commence to demonstrate the downstream fiber resorting process. The A and B positions might reverse, depending on whether the paradigm's impact causes retardation or acceleration (see Section 4.2.4). (b) The graphics on the left side show a series of schematic stills depicting five developmental stages down the cascade of the long primary afferent system's assembly line (see Figure 2b(1–5)). The colors reflect the current dominating stages of developed axons (see the legend in Figure 1 for more details). On the right side, the line graphics show axons from individual neurons at DRG L4-L6, represented as pars pro toto. The critical period delineates the upstream period of axon elongation at spring tide (green line). Beyond this, all of the long primary afferent axons have reached their targets and continue developing down the cascade. The graphic at the bottom (see Figure 2b(6)) shows the final stage of the two subdivisions of the long primary afferent system originating from separate neurons in three lumbar DRGs. The pioneering TH.0-staged axons target the gracile nuclei in high-tide waves at spring tide. Next, successive TH.0-staged axons in low-tide waves target Clarke's nucleus at neap tide. The color variations reflect the stages in which the axons have transitioned thus far.

The high-tide TH.0-staged fibers might be quite energy-demanding. In terms of waves, the f-ES might reflect accumulated energy, figuring the spring tide at the medulla. Its mimicry was assigned to the a-FS abutting the rostral lesion site at an upstream M_0 . The compact bundle of DC axons readily disclosed the a-FS. The neonatal configuration challenged the identification of individual axons in caudal Txs, causing imperceptible cut axons to terminate at variable distances from the lesion site. The adult configuration uncovered the i-FSs exhibiting the neap tide in low-tide axons. In Section 3.1.3, we address the ripening neuropil's confounding features, demonstrating interference with the development of Clarke's nucleus. The a-FS and i-FSs exemplify the two extremes of the upstream temporospatial developmental tempo of the long primary afferent axons.

Moreover, those features indicated a gradual decrease in the developmental tempo while stepping down the cascade. The low-tide axons might develop slower. They manifested in the caudal lesions, causing numerous i-FSs in adult cases. At spring tide, rostral Txs caused the a-FSs, which contained less than 50% of cut axons. The swift f-ES, graphically depicted in Figure 3a, might account for this limitation, corresponding to the higher developmental tempo. The M_0 s being random, capturing two a-FSs in a narrow time window in neonates, yielded an incidental finding. Figure 3b depicts the low-tide axons targeting Clarke's nucleus at a lower tempo. The low thoracic Txs caused i-FSs distanced from the lesion site. Notably, the number of axons and time lapses were unquantifiable.

The paradigm's impact on normal development.

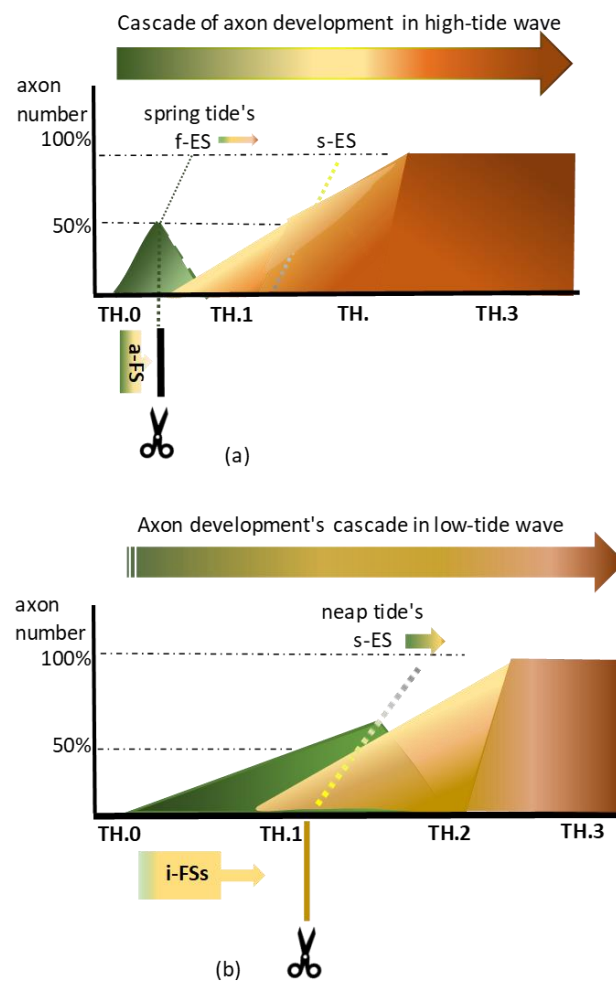


Figure 3. (a): Rostral Txs of the fast-developing high-tide waves might yield less than 50% of axons cut while targeting the gracile nuclei. At spring tide, the hypothetical fast elongation stop (f-ES) might have accounted for the swiftness of the process, which shortens the timelapse of the pioneering high-tide axons arriving at the medulla. The upstream abrupt front stop (a-FS) rendered by a Tx at a rostral level mimicked this hypothetical phenomenon. At upstream M_0 , a Tx might have yielded less than 50% of cut pioneering axons when the TH.0 stage took a short time. After cutting, the a-FS abutted the caudal margin of the lesion site. The tracer, visible up to the fiber tip, underpinned the axon repair, favoring the axon's vitality. (b): Caudal Txs of low-tide axons caused numerous i-FSSs, which may reflect a slow elongation tempo facing the s-ES. At neap tide, the chance of cutting more TH.0 staged axons may be greater than at spring tide. The cut low-tide axons created features of multilevel individual front stops (i-FSSs). They mimicked the hypothetical slow elongation switch (s-ES) phenomenon at the medulla. After that, all pioneering axons might have begun accommodating their elongation speed to the slow spinal cord's growth before forming collaterals into gracile and Clarke's nuclei. At this slower process, a caudal Tx might have yielded over 50% of long primary afferent axons from both subdivisions.

3.1.3. The Low-Tide Waves and the Neuropil's Ripening

The i-FSSs located caudally from the lesion sites in the adult experiments were related to Clarke's nucleus and hampered development. The representation of the nucleus relied on the randomly acquired signs of inferred neurogenesis, which added to the neuropil's circumferential growth at the upstream M_0 s. Figure 4 shows the graphics of the primordial upstream and regular downstream assemblage. The upstream low-tide axons joining the dorsally pioneering high-tide axons fail to target Clarke's nucleus. The unripe neuropil, preventing the low-tide TH.0-staged axons from penetrating, remains blank. Despite

neurogenesis and dorsal horn growth, the low-tide TH.0-staged axons might stick to a dorsal trajectory.

In contrast, having targeted Clarke's nucleus, the attached short-length colls might lengthen following Clarke's nucleus, showing a passive shift down the DC. Lengthy colls traversed the DC-WM through its depth, penetrating the ventral targets in mid-sagittal sections. Spinal cord development yielded short and long straight or oblique trajectories. Section 4.2.1 argues that low-tide axons may form these colls. Those multilevel colls along the spinal cord related to concealed dynamic mechanisms were disclosed after TxS. The neuropil's ripening state determined the extensiveness of Clarke's nucleus. In the controls, a well-formed nucleus extended up to a mid-thoracic level in Rexed layer VII at either side of the central canal [23].

Hyposaturation linked to the paradigm might have retarded normal development. The neuropil with a finely tuned ripening ahead of the penetrating colls from the low-tide axons might have been dissociated. The impervious neuropil prevented the axons' colls from penetrating Clarke's nucleus. After TxS, the sequelae of this two-edged impact yielded confounding configurations of the temporospatial development of both interlinked systems. The trajectories of the high-tide long primary afferent axons were the easiest phenomenon to identify. The low-tide axons, sharing a common pathway, elucidated a superimposed effect of hypertrophy on Clarke's nucleus. This understanding, assessed from the neuropil's delayed ripening, is first depicted graphically in Figure 4 (see below) and Figure 18.

The primordial (a) and Clarke's nucleus-embedded neuropil ripened in due course (b).

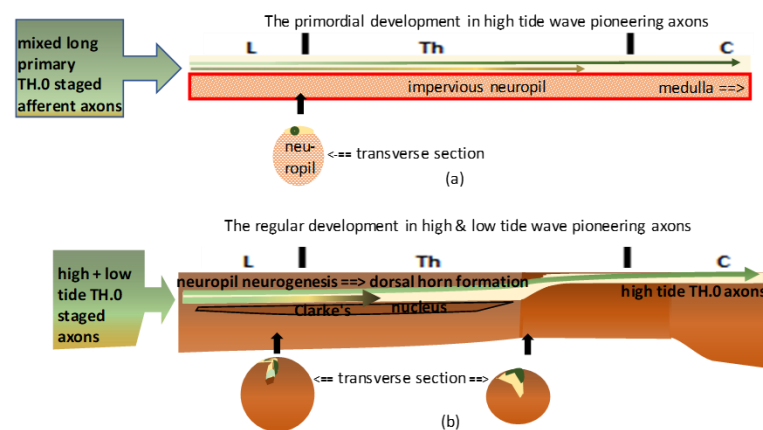


Figure 4. (a): The graphic shows the primordial assemblage. The most upstream TH.0-staged pioneering long primary afferent axons were the first identifiable high-tide axons to cover the immature neuropil dorsally (dark green line). The low-tide axons (light green line) might have reached upper thoracic levels, intermingling with high-tide axons before Clarke's nucleus manifested its anlage. (b): The graphic shows the natural temporospatial assemblage in duly ripened neuropil. Dorsal horn (DH) formation might have pushed down the high-tide axons and the low-tide axons connected with Clarke's nucleus. DH overgrowth delineated Clarke's nucleus in its rostral extent, which might have varied in length. Beyond the uppermost level, the TH.0-staged axons remained at the initial dorsal location, leveled with the gracile nucleus at the medulla.

3.2. Tx Related Perturbations

3.2.1. The Abrupt Front Stop of High-Tide Axons in Neonates

The neonatal cases show the most dynamic features, while the adult cases (see Section 3.2.2) are pivotal in assessing the difference between high- and low-tide dynamics. The left graphic on top of each picture offers a quick overview. Sensing the dynamics of the multistage axons just before the Tx, the long primary afferent system's dominant features graphically highlight the temporospatial development at the M_0 . The right graphic shows individual axons as pars pro toto from DRG neurons exhibiting the developed state after the Tx. The dynamic features at upstream M_0 s exhibited variability in response to

trauma. We classified the axons bypassing the lesion site as TH.0-staged axons pioneering up to the medulla. Those axons transitioned into TH.1 and TH.2. The first three neonates documented the final stage of unhindered coll formation within the gracile nucleus.

The first neonate, M_0 : E16.p7, with a low thoracic Tx, offered details of an upstream M_0 , considering the labeled gracile and Clarke's nucleus (Figure 5). The involved high-tide TH.0-staged axons could have crossed the lesion site. The labeled left gracile nucleus exhibited spotty blank areas (Figure 5f). These might relate to high-tide previously cut TH.2-staged axons, originating from the most rostral DRG neurons, i.e., possibly L4. The Tx at the level of Clarke's nucleus rendered the cytoarchitecture in disarray. The colls had targeted the local neuropil. The label at either side of the midline confirmed the disruption of the dorsal septum (Figure 5d). Beyond the upstream cut high-tide axons, the low-tide TH.3-staged axons might have contributed to label enhancement (Figure 5d). The oblique colls nearby and straight colls further caudally from the lesion site labeled Clarke's nucleus and its anlage (Figure 5c,d). The coll formation extended beyond the lesion site at upper thoracic levels. Downstream unharmed TH.0-staged axons might have formed these colls, which are considered dystopic at these rostral spinal levels (Figure 5e).

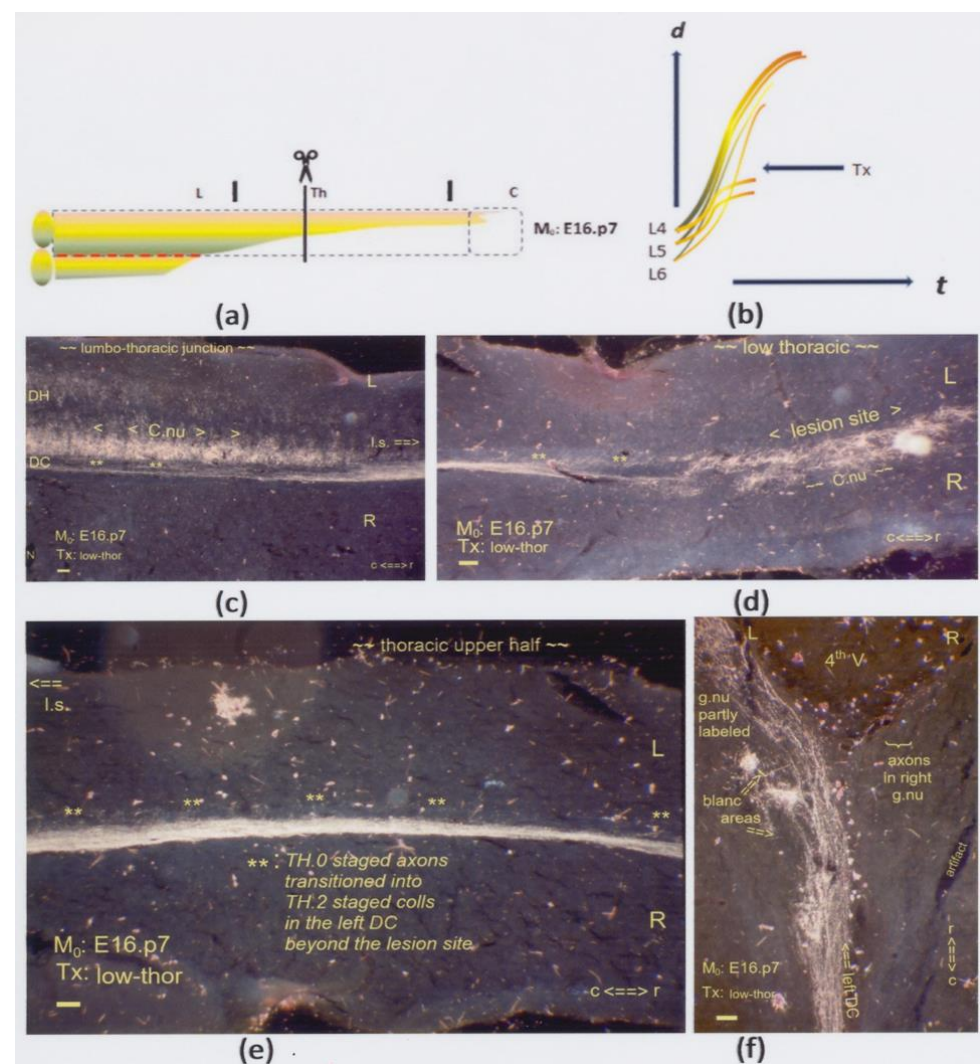


Figure 5. (a,b) The graphics show a low thoracic Tx at M_0 : E16.p7. The interrupted red line indicates the possible inaccessibility of the neuropil, affecting the development of Clarke's nucleus. Shown here are horizontal sections. (c) At the lumbo-thoracic junction's level and halfway through the dorsal horn (DH), the left dorsal column (DC) contains the long primary afferents labeled with antegrade transported HRP. Some label enhancement of Clarke's nucleus might be due to retrograde degeneration

in cut TH.3-staged fibers of the long and intermediate subdivisions. The fibers radiated in straight and oblique TH.2-staged long colls (tandem asterisk: **). (d) The Tx damaged the anlage of Clarke's nucleus with an impact on its cytoarchitecture at either side of the midline. TH.2-staged colls (**) targeted the local neuropil. The bilateral features of the Tx indicated a twofold dynamic feature: any TH.3-staged cut axon growing into the lesion site might as well have crossed the midline. (e) Unharmful downstream pioneering TH.0-staged axons transitioned into TH.2 colls (**) rostrally beyond the lesion site at upper thoracic levels. (f) Fully developed TH.2-staged colls labeled parts of the left gracile nucleus. Spotty areas remained blank. The Tx revealed that upstream-staged axons bypassed the lesion, while cut axons might explain the blank spots. All scale bars: 100 μ m.

For comparison purposes, the control experiments exhibited the features of gracile and Clarke's nuclei (Figure 6a,e,f). In contrast with Figure 5f, the label in gracile nucleus was spread evenly (Figure 6a). Figure 6b,c depict the CG exhibiting features of the short subdivision, which was beyond the scope of our research. The labeling at DREZ levels manifested gradually and concomitantly in the experiments down along the cascade [22].

Left sciatic nerve tracing features of the D(V)REZ, Clarke's nucleus, and gracile nucleus in one neonate and two adults.

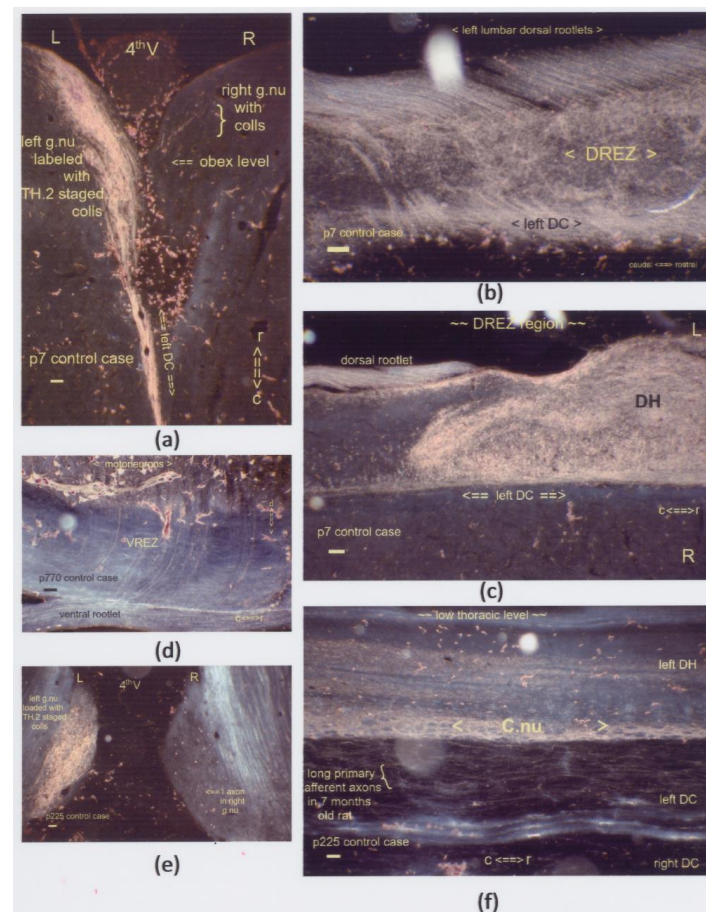


Figure 6. Tracing features of the targets in control experiments without Tx are shown for comparison to the experimental results. (a–c) In a p7 neonate, the left gracile nucleus was fully labeled by antegrade transport of HRP. The right nucleus also featured some TH.2 colls. The DREZ region and the DH featured characteristic labeling. On display are horizontal sections, except the sagittal section in (d). The lumbar VREZ depicts individual axons and motoneurons in an almost two-year-old rat. (e) The left gracile nucleus exhibited a clear label in a seven-month-old rat. (f) Also, an axon-built gossamer is shown in the left DC adjacent to Clarke's nucleus. Notably, a longer follow-up morphed the features on display (d,f).

The second neonate, M_0 : E16-8h.p8, displayed a cervical lesion site (Figure 7). A dorsal hump marked the lesion site, demonstrating neuron excess for almost two weeks. The white matter facing abrupt front stop (a-FS) was a stack of the high-tide wave axons abutting the dorsal humped lesion site (Figure 7e). This stack at the dorsal surface and downstream TH.0-staged axons leveled properly with the gracile nucleus. Ventrally, pioneering axons crossed the neuropil, and a few reached the medulla. Figure 7f shows the penetrated gracile nucleus. Several TH.2-staged axons also exhibited colls within the hump and into the ventral neuropil. Figure 7c,d shows unique features of random target-bound long colls spread throughout the mid and upper thoracic DC. In Figure 7c, the colls exhibit the rostral extent of the upstream anlage of Clarke’s nucleus with a location halfway through the dorsal horn reflecting its primordial state.

Considering the colls in Figure 7d, the contribution to Clarke’s nucleus with a rostral extent up to the thoracic–cervical junction might seem questionable. A comparison between the M_0 s of the p7 and p8 neonates shows that the p7 neonate’s graphic colors are greener, depicting TH.0-staged axons labeling the gracile nucleus after the Tx. The M_0 fell upstream on the assembly line. The M_0 of the p8 neonate’s Tx might have fallen downstream, creating the final spring tide axons with transitioned colls within the gracile nucleus (Figure 7f). These neonates illustrated the opposite states regarding the development of Clarke’s nuclei. The p7 case demonstrated the advanced maturity of Clarke’s nucleus compared to the primordial features in the p8 neonate. It is noteworthy that the M_0 denoted by the day appeared inaccurate in pinpointing M_0 ’s spot at the cascade where Clarke’s nucleus is concerned.

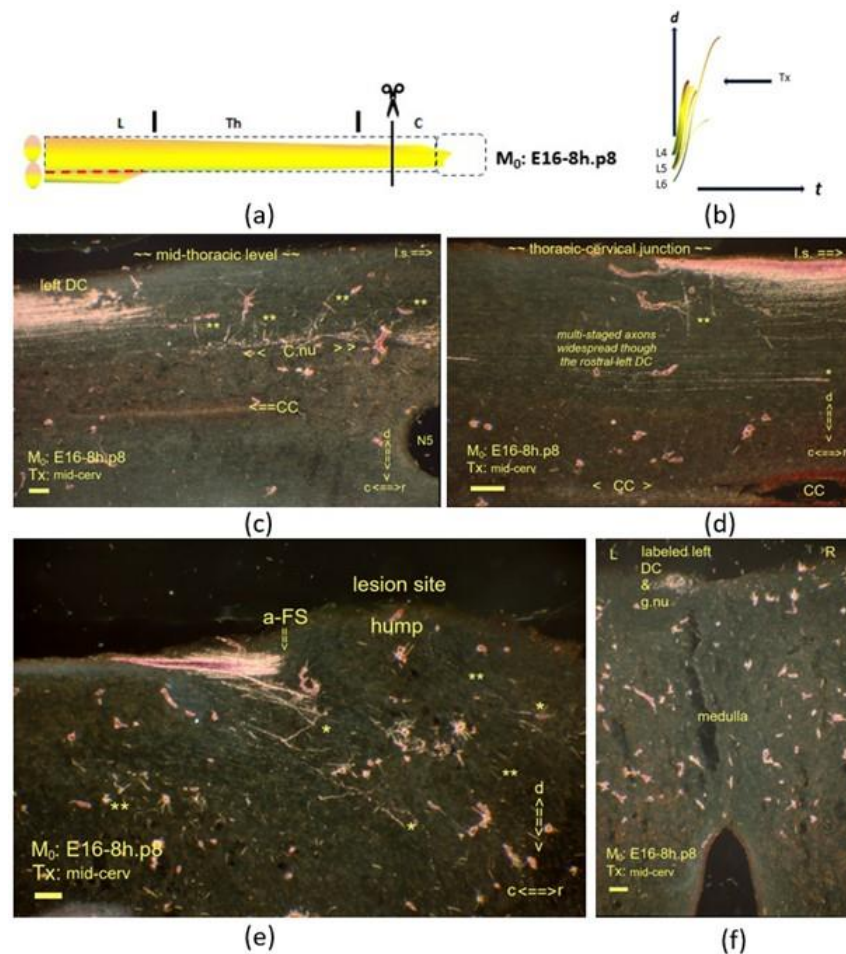


Figure 7. (a,b) The graphics show a mid-cervical Tx at M_0 : E16-8h.p8. The interrupted red line

is explained in the caption of Figure 5. Sagittal sections are displayed, and a horizontal one is shown in Figure (f). (c) Mid-sagittally, the compacted label shows multistage axons in a bundle. Given the CC is centered almost in the middle, the anlage of Clarke’s nucleus was hypotrophic and located dystopically halfway through the DH. The tandem asterisk (**) marks the TH.2-staged long colls and oblique colls. (d) One asterisk (*) marks the TH.1-staged i-FS caudally from the lesion site. The few colls (**) document a dystopic level at the thoracic–cervical junction. The widespread multistage long primary afferents throughout the depth of the DC question whether the DC harbored high-tide axons exclusively at this dystopic rostral level. (e) The fiber stack of TH.1-staged axons exhibited an abrupt front stop (a-FS), mimicking the hypothetical fast elongation stop (f-ES) phenomenon at the medulla. The lesion site featured multistage axons. Some had crossed the lesion site, considering the labeled gracile nucleus. (f) Those fibers had transitioned into the TH.2-staged colls and penetrated the left gracile nucleus. All scale bars: 100 μ m.

The third neonate, M_0 : E16.p4, displayed a low thoracic lesion site with the disturbed anlage of Clarke’s nucleus (Figure 8). Clarke’s nucleus exhibited an abundant label at the lumbo–thoracic junction level, comparable to the p7 case. At the lesion site (see Figure 8d,e), the TH.2-staged colls combined with TH.3-staged axon terminations in the fringe might have enhanced the label. The final fibers (Figure 8f) featured spring tide axons at both sides of the medulla. The same axons might have remained subpially, having crossed the lesion site (Figure 8c–e).

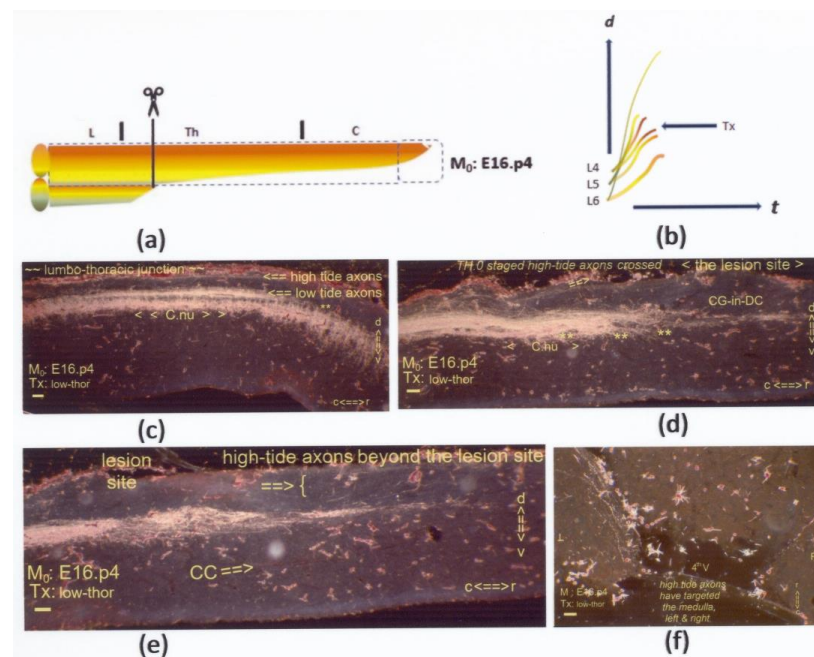


Figure 8. (a,b) The graphics show a low thoracic Tx at M_0 : E16.p4. Sagittal sections are on display, except for (f), which is horizontal. (c) At the lumbo–thoracic junction, Clarke’s nucleus featured quite an intense labeling pattern despite its probably dystopic, overly dorsal location. Considering the label in the gracile nucleus, the subpial axons are identified as the final high-tide pioneering axons at spring tide. (d) Most likely, the same high-tide fibers followed this subpial trajectory, distinct from the ventral dominant fiber bundle harboring multistage axons. They terminated in the local neuropil at the lesion site marked by the CG-in-DC feature. Potentially, cut TH.2- and TH.3-staged high- and low-tide axons might have accounted for the hyperintense label that featured enhancement just caudal from the lesion site. The tandem asterisk (**) indicates colls (c,d). (e) A 40 μ m shift to the midline at the lesion site depicts the upstream axons, which crossed the lesion site. The three slides indicate a tendency for circumferential growth of the DH, relating to a ventral migration of Clarke’s nucleus. (f) At spring tide, these few fibers in the DC managed to target the medulla. All scale bars: 100 μ m.

In these three neonates, the neuropil showed variable accessibility at upstream M_0 s. An overt primordial state of spinal cord tissue appeared when it was almost inaccessible (see Figures 14 and 15).

The fourth neonate, M_0 : E16-9h.p6, displayed another Tx beyond Clarke's nucleus (Figure 9). The upstream Tx's rostral level caused another a-FS in the series. This configuration of bundled TH.1-staged high-tide axons supposedly mimics the f-ES, i.e., the hypothetical transition at the medullary's targets. The features of Clarke's nucleus might parallel the spinal cord's ripening state (Figure 9c). The small TH.3-staged CG-facing FS, caused by high-tide cut axons, underlined a downstream drift (Figure 9e,f). The overabundance of bilateral dystopic high-tide colls also reflected developmental progress down the cascade (Figure 9d–f). The gracile nucleus was devoid of the label.

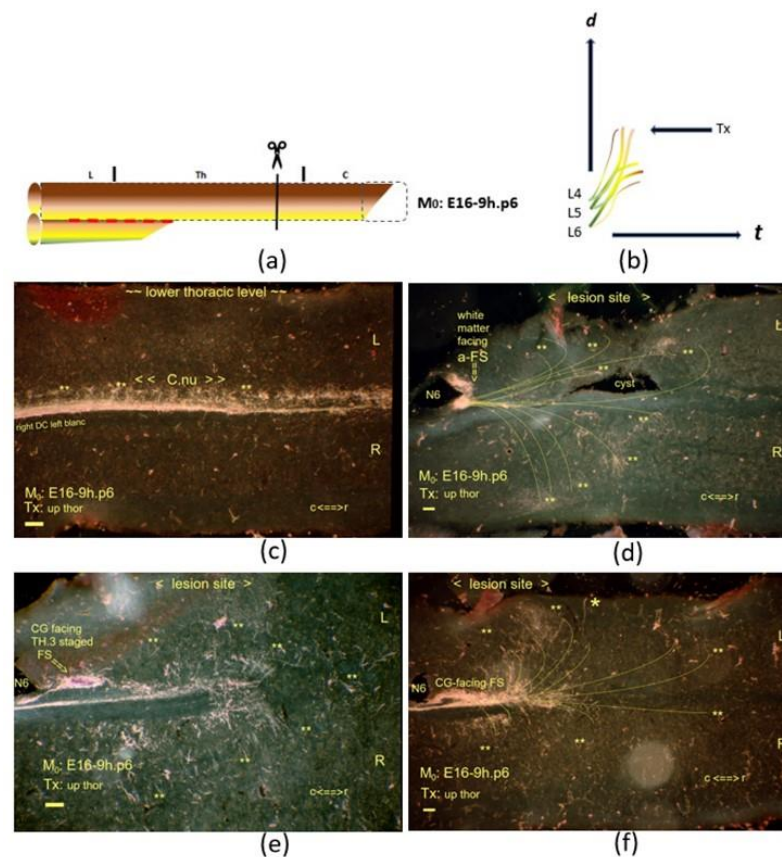


Figure 9. (a,b) The graphics show an upper thoracic Tx at M_0 : E16-9h.p6. The interrupted red line indicates the neuropil's inaccessibility, affecting the development of Clarke's nucleus. On display are horizontal sections. (c) At a one-hour upstream M_0 , Clarke's nucleus featured advanced ripening compared to the nucleus in the E16-8h.p8 neonate displayed in Figure 7c. (d) The lesion site involved multistage fibers with an a-FS caudal from the traumatic cyst. TH.2-staged colls (**) traversed the neuropil on either side of the lesion site. The N6 iron fix pin has split the a-FS. (e) The small CG-facing FS, just rostral to the pinhole, was another downstream stage indicating a drift down the cascade. The TH.3-staged axons were close to the a-FS axons, which abutted the caudal border of the lesion site, marked with the N6 fix pin. (f) Beyond this level, the axons exhibited dynamic features of many TH.2-staged colls penetrated deep into the neuropil (d–f). The gracile nucleus devoid of the label also confirmed the developmental progress compared to the former p8 neonate. All scale bars: 100 μ m.

3.2.2. The Individual Front Stops of Low-Tide Axons in Adults

Txs at the upper thoracic spinal level could differentiate the high from the low-tide axons. In neonates, i-FSs were imperceptible. The rostral thoracic Tx caused the neonatal a-FS of high-tide axons, camouflaging any caudal i-FS when present. The neonate's densely

labeled stack of fibers became age-morphed, transforming into the perceptible i-FSs displayed at thoracic levels in adult cases (Figures 10 and 11). In contrast with the rostral a-FS, the peculiar configuration of the caudal i-FS might have reflected a less dynamic property. After Tx, the axons also recuperated but terminated caudally from the lesion site. This feature mimics the speculative s-ES, just like the a-FS might have mocked the f-ES. The i-FS and a-FS features manifested the blocking mechanism of the neuron’s development at the assembly line and delineated their critical periods.

The first adult case, M₀: E16-3h.p145, displayed an upper thoracic lesion site (Figure 10). Compared to the last p6 neonate, the M₀ fell six hours later. However, the developmental states of the long primary afferent systems shared similarities. The little fiber bundles terminating at two opposite CG-facing FSs of TH.3staged axons (Figure 10e,f) look comparable to the one shown in Figure 9e,f. Numerous TH.1-staged axons showed the multilevel i-FSs scattered throughout the lower thoracic DC (Figure 10c). These axons captured caudally at their neap tides might have been related to the tentatively inaccessible caudal neuropil. The age-morphed high-tide axons built an a-FS abutting the rostral lesion site (Figure 10e). The gracile nucleus was devoid of the label.

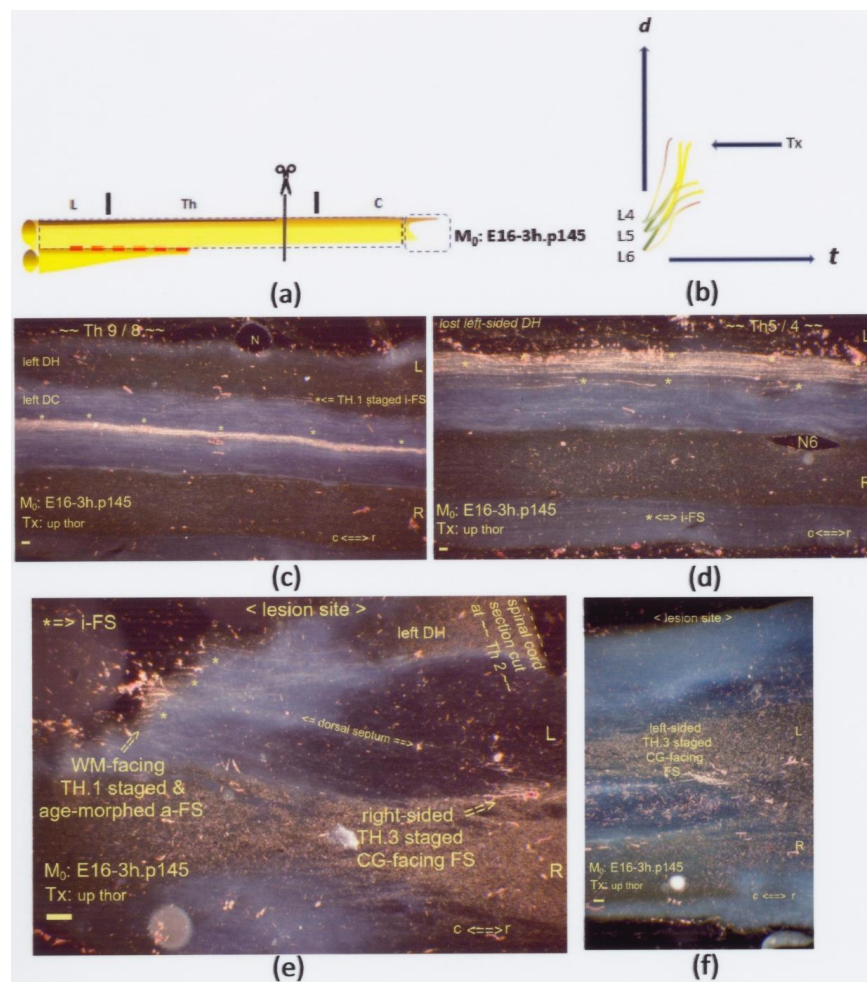


Figure 10. (a,b) The graphics show an upper thoracic Tx at M₀: E16-3h.p145. The interrupted red line indicates a possible state of dissociated neuropil. On display are horizontal sections. (c,d) Numerous multilevel i-FSs (marked: *) were captured mid-sagittally at levels caudal from the lesion site. Their visibility was due to age morphing. (e) Also, i-FSs were visible, constituting an age-morphed WM-facing a-FS marked with three single asterisks (*) in a row across the DCs. The Tx created multistage axons. This lesion site entailed two central gray-facing FSs. The TH.3-staged axons terminated at bilateral fringes. This FOV depicts one FS at the contra-lateral side, confirming a Tx. (f) Halfway down the left DC, the ventral location shows another tiny CG-facing FS. All scale bars: 100 μm.

The second adult case, M_0 : E16-1h.p240, displayed a mid-thoracic lesion site (Figure 11). The abundance of mid-sagittal i-FSs at a lower thoracic level was the dominant feature (Figure 11c,e). The Tx-rendered features were comparable to the horizontal section of the p145 adult, despite a difference of two hours between their M_0 s. The TH.3-staged FS, assigned to high-tide pioneering axons, marked the lesion site caudally (Figure 11f). The numerous i-FSs, mimicking the slow elongation switch (s-ES) phenomenon in axons cut at the neap tide, documented a shift from a ventral to a dorsal trajectory (Figure 11c,e). The Tx had detrimental repercussions, e.g., hypotrophy of Clarke's nucleus (Figure 11d). The intercurrent delayed ripening of the neuropil was probably at stake here (see Sections 4.2.1 and 4.2.3).

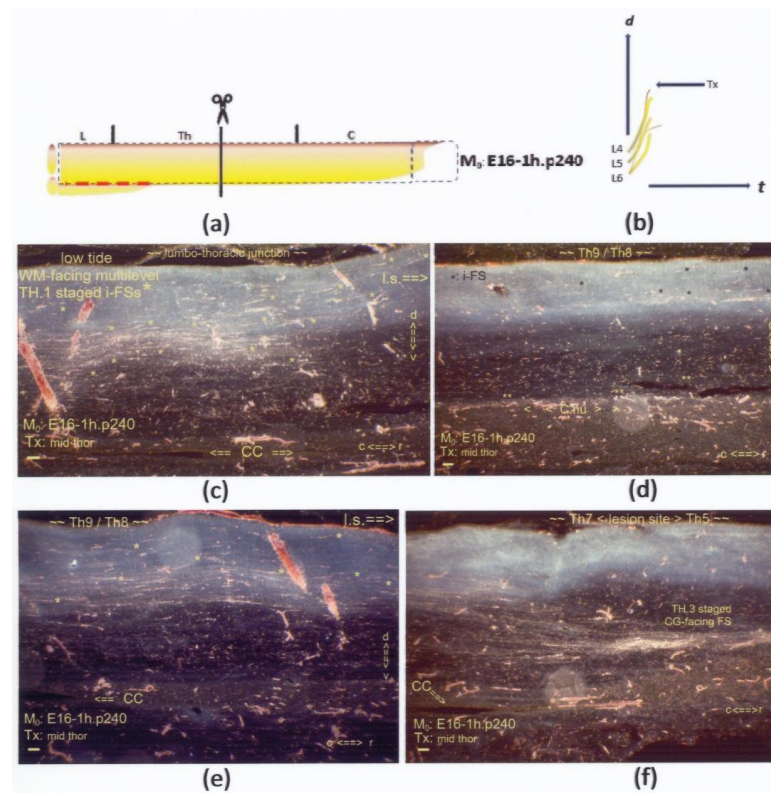


Figure 11. (a,b) The graphics show a mid-thoracic Tx at M_0 : E16-1h.p240. The interrupted red line indicates the neuropil's inaccessibility (v.s.). On display are sagittal sections. (c,d) Two slides, the first and the last of a series of four consecutive FOVs from the same mid-sagittal section, display the left DC at and near the midline. (c) Numerous mid-sagittal i-FSs (marked: *) had spread DC-wide at the lumbo–thoracic junction. The fibers turned from ventral to dorsal trajectories, acknowledged as mutual pathways for high- and low-tide pioneering fibers. Numerous i-FSs were identified as low-tide axons cut at their neap tides. (d) The tentative low-tide colls (marked: **) featured a delicate label at the fringe, suggesting a hypotrophic Clarke's nucleus. The underdevelopment of Clarke's nucleus might relate to the inaccessible neuropil due to delayed ripening, addressed in Section 4.2.3. (e) Still, more mid-sagittal i-FSs (marked: *) were scattered through the dorsal half of the DC. (f) A CG-facing FS identified the caudal border of the lesion site at a level of a few thoracic segments rostral to (e). The midline was nearby, given the CC. Compared to the tiny FSs in the p145 case, this FS might have harbored more high-tide TH.3-staged axons. The increment complied with the gradual downward shift, corresponding with the difference between the conception-bound M_0 s. All scale bars: 100 μ m.

The third adult case, M_0 : E16.p35, displayed a mid-thoracic lesion site (Figure 12). Like the last case, the caudal hypotrophic Clarke's nucleus exhibited feeble labeling at a dystopic location targeted by a few colls (Figure 12c,d). This state of development figured

an age-morphed configuration downstream from the neonatal state in Figure 9c. The dominant feature turned into aggregated multistage axons, which caused the CG-facing FS (Figure 12e,f). The hypotrophic Clarke's nucleus at its caudal part turned into label hyperintensity or enhancement due to the combination of TH.1-, TH.2-, and TH.3-staged axons at the mid-thoracic lesion site. The Tx had lesioned high- and low-tide axons in their dorsally kept common trajectory. The features indicated progress down the assembly line, as the FS entailed more TH.3-staged axons than the former p240 case. The wider FS might offer another example of midline crossing, as shown in the p145 case. Considering the exposed length of the CC (Figure 12f), the torn midline septum might gradually have yielded encroachment upon the other side.

The fourth adult case, M₀: E16-1h.p195, displayed a low thoracic lesion site (Figure 13). At the lumbo–thoracic junction, several long colls (marked: **) targeted Clarke's nucleus, which might have exhibited progressed ripening (Figure 13c,d). The CG-facing FS dominated the configuration (Figure 13e,f), featuring TH.3-staged axons, except for a single i-FS (marked: *). The axons aggregated into a presumable radicular pattern (Figure 13f). These characteristics might reflect decreased dynamic features near the end of the assembly line.

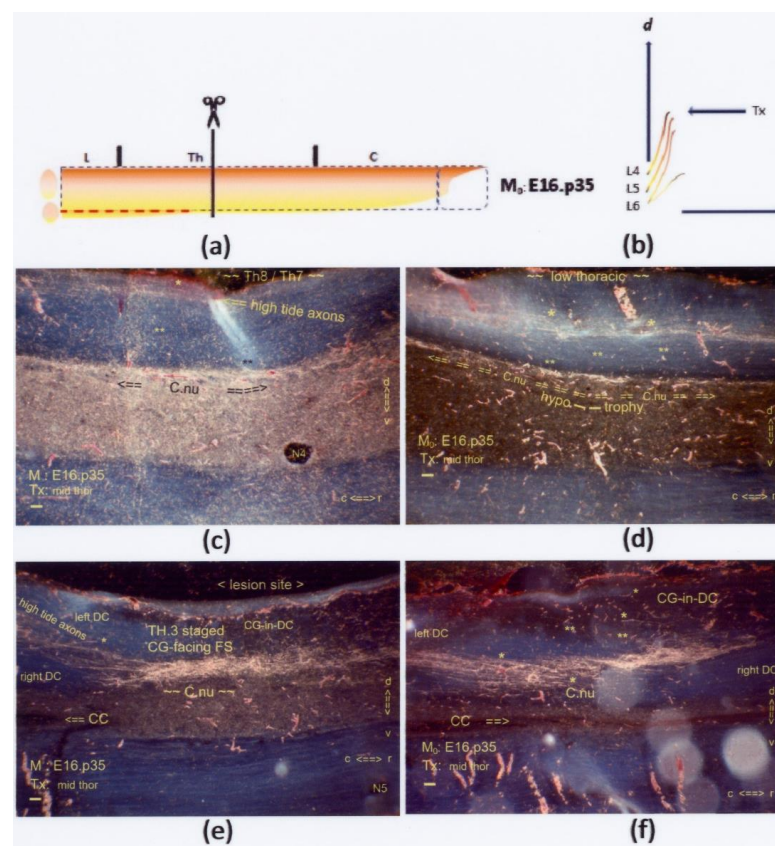


Figure 12. (a,b) The graphics show a mid-thoracic Tx at M₀: E16.p35. The interrupted red line indicates the neuropil's inaccessibility, related to a hypotrophic state of Clarke's nucleus. On display are sagittal sections. (c,d) Subpially and halfway down the DC, high-tide fibers elongated across the low thoracic DC. A few i-FSs (marked: *) were discernible. A few low-tide colls (marked: **) targeted a hypotrophic Clarke's nucleus at a dystopic, overly dorsal location. The configuration, morphed by age, might be comparable to the neonatal configurations of the primordial Clarke's nucleus in Figure 7c and Figure 14c. (e,f) Halfway through the DH, the CG-facing FS contained multistage axons, e.g., TH.1-, TH.2-, and TH.3-staged high- and low-tide axons. The few i-FSs and colls are marked * and **, respectively. Retrograde degeneration of cut TH.3-staged axons at the fringe might also have contributed to the label's enhancement. This Tx-rendered axon confluence might have encompassed Clarke's nucleus's disrupted anlage. All scale bars: 100 μ m.

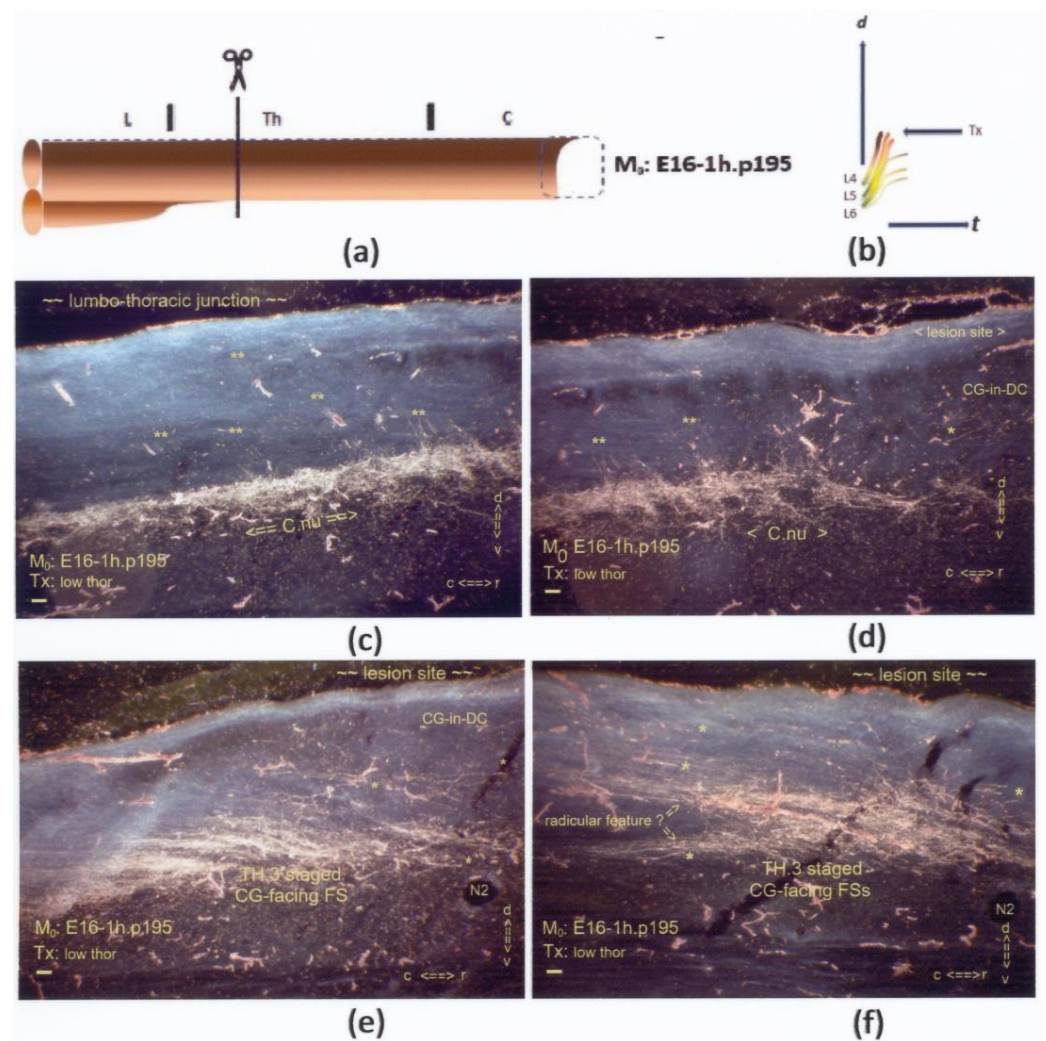


Figure 13. (a,b) The graphics show a low thoracic Tx at M₀: E16-1h.p195. On display are sagittal sections. (c,d) The first two consecutive slides show long oblique colls (marked: **) across the DC-WM, targeting a rather mature state of Clarke's nucleus at the lumbo–thoracic junction. (e,f) These two slides exhibit the caudal level adjacent to the lesion site at one FOV rostrally to the latter pair of slides. A few i-FSs (marked: *) are discernible. All slides depict left-sided sections. The TH.3-staged axons joined an extensive CG-facing FS on top of Clarke's nucleus. With the combination of all high-tide and many low-tide cut axons, the enhancement was a matter of course. All scale bars: 100 μ m.

3.2.3. The Primordial State and the Inaccessibility of the Neuropil

The developmental cascade was uncovered at random upstream M₀s when the Txs caused features to be ascribed to unknown phenotypes. The next three cases exhibited peculiar characteristics regarding the inaccessibility of immature neuropil. The features underlining the temporospatial development of the spinal cord's neuropil might dissociate from the long primary afferent axons.

The neonate, M₀: E16.p3, did not display any features of a detectable Tx at a low thoracic level (Figure 14). Halfway down the DH, the poorly labeled anlage of Clarke's nucleus showed hypotrophy (Figure 14c,d). Acknowledging the high- and low-tide concept, the few colls involved are classified as downstream low-tide TH.2-staged axons. Regarding its known location in Rexed layer VII close to the central canal, this dystopic location halfway down the DH might indicate that these pioneering axons were the last low-tide axons which targeted the anlage. Many TH.0-staged pioneering axons had crossed the lesion site. Accordingly, high- and low-tide intermingled TH.0-staged axons might have transitioned into DC-WM colls in the upper spinal cord, illustrating the neuropil's

inaccessibility (Figure 14e). Many colls penetrated the ventral neuropil, opposite the gracile nucleus's dorsal location (Figure 14f). Tentatively, among these long colls, some might have transitioned from low-tide axons, which penetrated the ventral neuropil dystopically (see Section 4.2.4).

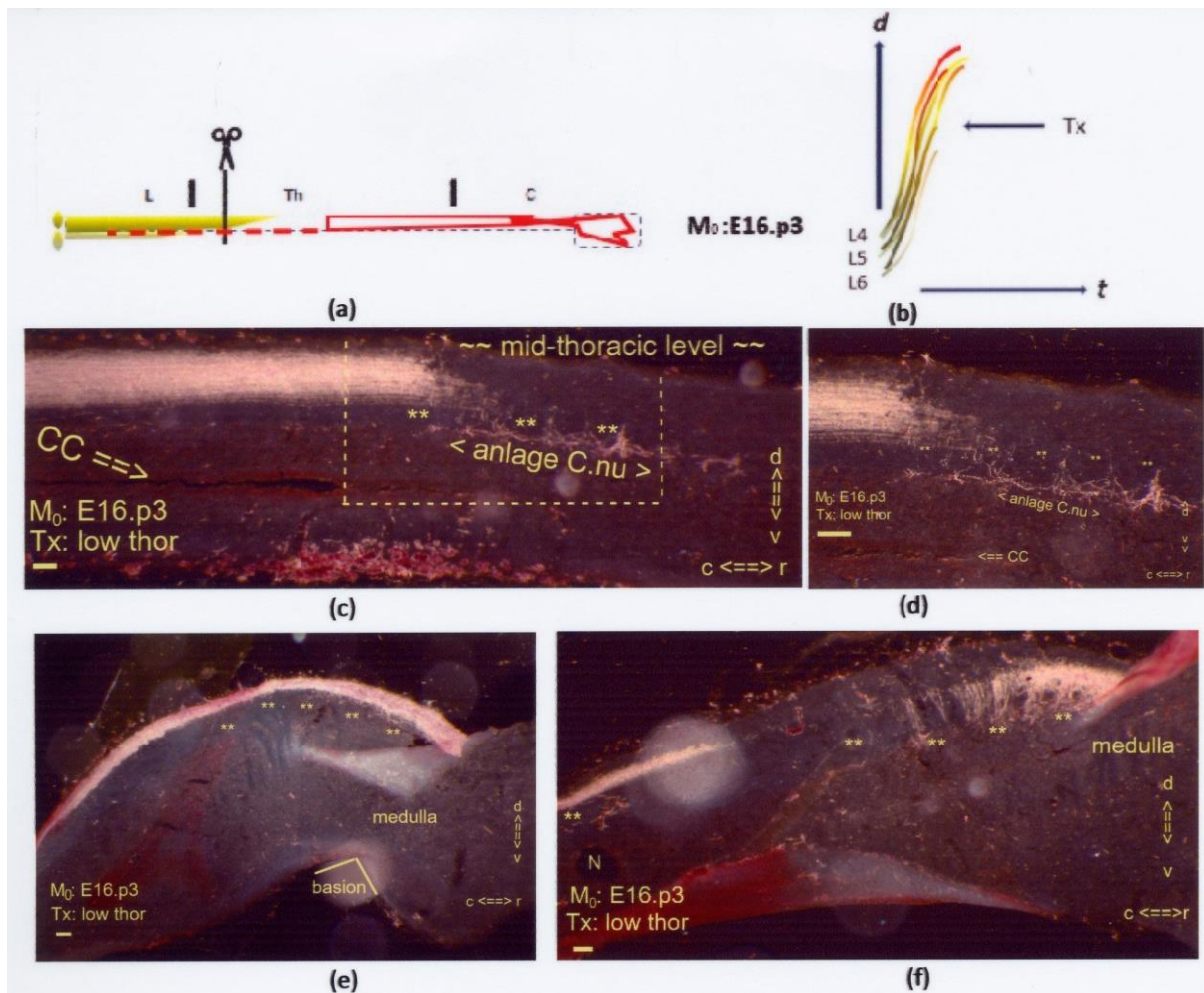


Figure 14. (a,b) The two graphics show a low thoracic Tx at M_0 : E16.p3. The interrupted red line indicates the few low-tide axons targeting Clarke's nucleus next to a possible increased number of long primary afferents in the rostral DC (uninterrupted red line). On display are sagittal sections. The Tx caused an indiscernible lesion site. (c,d) The dystopic anlage of Clarke's nucleus featured hypotrophy at the mid-thoracic level with colls (marked: **). The boxed area duplicates at higher magnification in Figure 14d. (e) Dystopic long colls in DC-WM (marked: **) were visible in the cervical region near the medulla. (f) Multilevel long colls (marked: **) crossed the depth of the DC and penetrated the neuropil caudal from the medulla. The configuration was at variance with the position and level of the gracile nucleus located at the dorsal medullary surface. Hypothetically, the long colls might be considered target-bound low-tide axons. All scale bars: 100 μ m.

The young adult, M_0 : E16+2h.p40, displayed an upper thoracic lesion site (Figure 15). An inconspicuous CG-in-DC feature marked the lesion site (Figure 15c). The DC harbored multilevel, i.e., dystopic, colls traversing the DC-WM (Figure 15d–f). Numerous colls had penetrated the fringe, suggesting impervious neuropil and indicating dissociation by example. The partly labeled gracile nucleus (Figure 15g) exemplified the impact of the Tx on cut axons, which might be responsible for the blank areas of the gracile nucleus.

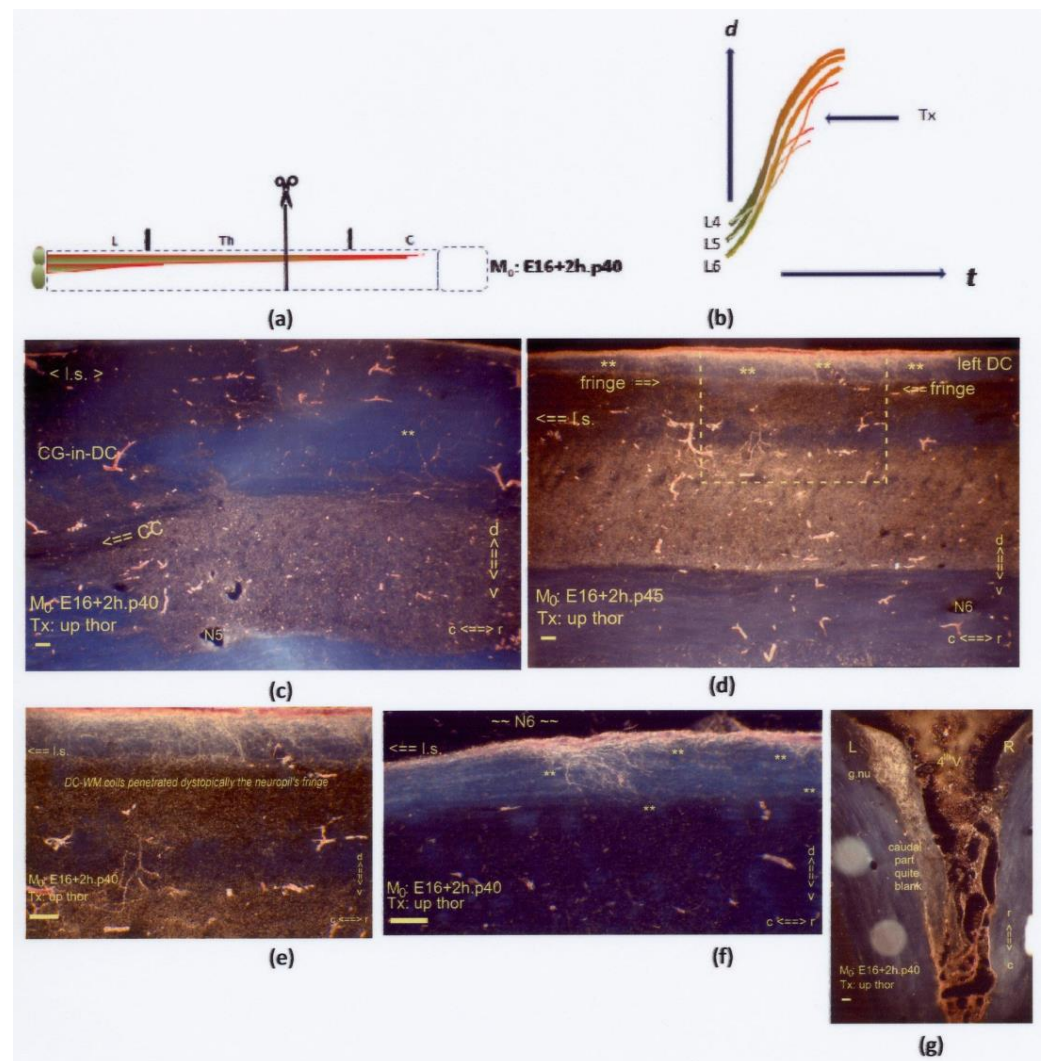


Figure 15. (a,b) The two graphics show an upper thoracic Tx at M_0 : E16+2h.p40. The uninterrupted red line delineates the almost inaccessible neuropil. Sagittal sections are displayed, except for (g), which is horizontal. (d,e) Rostrally to the lesion site in (c), DC-WM colls (marked: **) had developed and penetrated the ventral fringe scantily. The development of these axons was dystopic regarding the upper thoracic levels. (d) The dystopic colls (marked: **) are located beyond the lesion site (l.s.). The boxed area is duplicated at higher magnification in (e). (f) Some colls (marked: **) wandered aimlessly within the DC-WM at an upper thoracic level rostral to the lesion site (l.s.). (g) After the Tx, high-tide TH.0-staged axons pioneered the DC and transitioned into the colls, which labeled the rostral part of the left gracile nucleus. The caudal half of the nucleus remained almost blank. All scale bars: 100 μ m.

The neonate, M_0 : E16+7h.p9, displayed features after an undetectable Tx at an upper thoracic level (Figure 16). The gracile nucleus on the right side contained an axon excess (Figure 16g). This paradoxical feature supposedly indicates a Tx. The many axons at the right gracile nucleus might reveal midline crossing at the indistinguishable lesion site. Multilevel colls scattered throughout the caudal neuropil are attributed to Clarke's nucleus's anlage (Figure 16c,d). The dystopic colls were present up to the cervical–medullary junction (Figure 16f). These dystopic colls confirmed an upstream state of development at its M_0 . The configurations might underline that the long primary afferent system development had continued after the Tx caused seemingly normal features, as far as Clarke's and the gracile nuclei were concerned. This M_0 fell slightly upstream compared to the first p7 neonate, which showed fewer TH.0-staged axons growing up to the gracile nuclei.

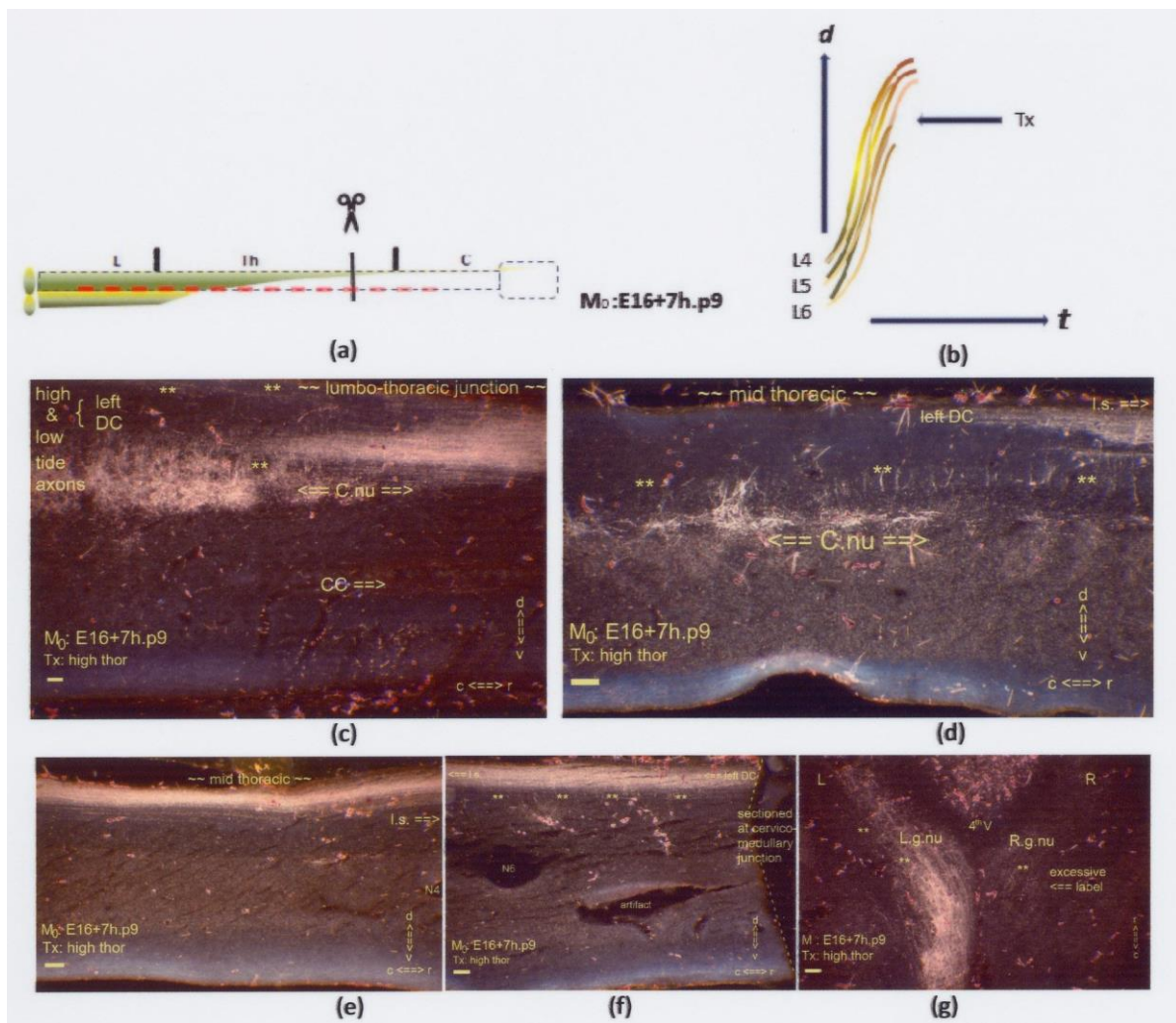


Figure 16. (a,b) The two graphics show an upper thoracic Tx at M_0 : E16+7h.p9. The interrupted red line indicates hampered penetration of the caudal neuropil. Sagittal sections are displayed, except for (g), which is horizontal. (c–f) Four slides encompass the spinal cord from the caudal to its thoracic extent. Numerous Th.2-staged colls (marked: **) are at the upper thoracic spinal cord. The lesion site was undetectable. (c) The intermediate gray showed multilevel labeled colls at a location distanced from the CC. (d) The rostral anlage of Clarke's nucleus was located too dorsally. (e) The high- and low-tide axons might have joined the uniform bundle in the DC. (f) The multilevel colls near the thoracic–cervical junction might contain tentatively dystopic low-tide axons. (g) The gracile nuclei were labeled abundantly by the colls (marked: **), like the lumbar neuropil in Figure (c). The richness of the label on the right side illustrates that the left-sided axons might have contributed to the labeling of the right gracile nucleus, confirming a fetal Tx, though undetected. The features justified classifying a neuropil's primordial state, illustrated graphically in Figure 18a. All scale bars: 100 μ m.

The latter three cases indicated a possible variability in the ripening of the neuropil, affecting the long primary afferent system's development. Clarke's nucleus suffered a most pronounced superimposed effect from the temporospatial dissociation. The different developmental conditions created confounding configurations of axons that were hard to classify.

3.2.4. The Hypotrophic Clarke's Nucleus at the Impervious Neuropil

At upstream M_0 s, the Txs could cause a proportional shift between the high- and low-tide axon development. The data showed that elongating high- and low-tide axons might

follow the same trajectory. The multilevel, TH.2-staged WM-colls in the upper thoracic DCs indicated reciprocity, i.e., a common or dichotomous pathway. The multilevel i-FSSs in the caudal thoracic spinal cord revealed the Tx-blocked development in low-tide axons, terminating caudally from the lesion site. The improper development of Clarke's nucleus, i.e., the hypotrophy, also paralleled the variability of its rostral extent. These findings from a complex cytoarchitecture under construction were challenging to interpret. The graphics depict the characteristics of the Tx-rendered developmental shift, as shown in Figure 17.

The direct Tx effect at hypoxia's two-edged impact on the long primary afferent system's development.

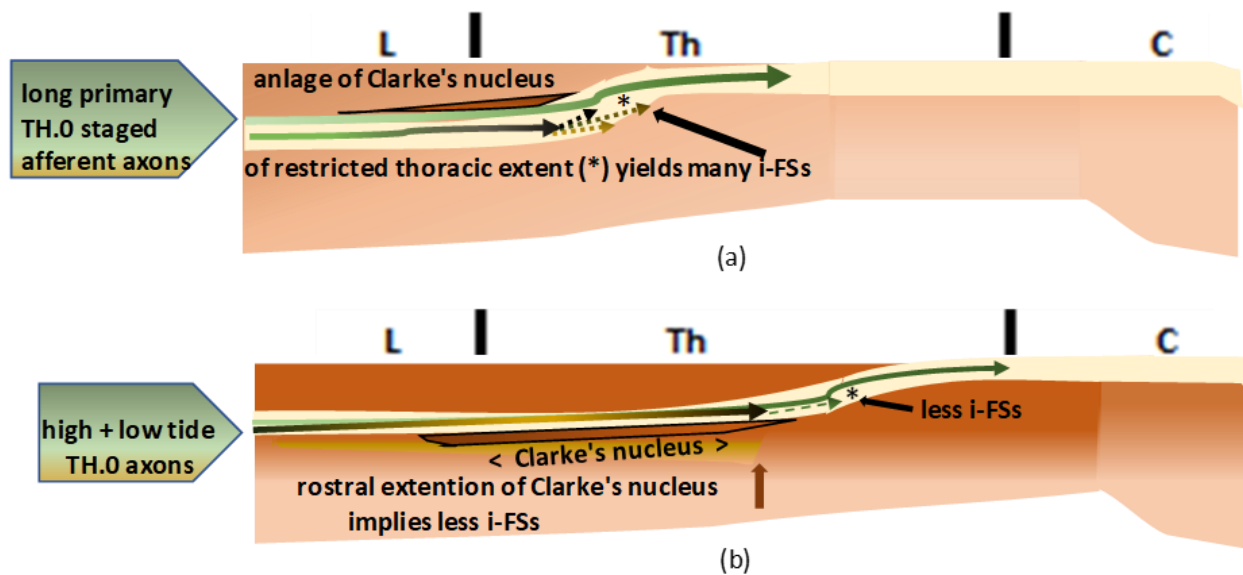


Figure 17. (a) At the upstream M_0 , the long primary afferent low-tide axons showed a dystopic anlage of Clarke's nucleus halfway down the DH. The adult cases showed the Tx-rendered i-FSSs (marked: *), which precluded the axons from targeting Clarke's nucleus. The mutuality between the high- and low-tide axons' trajectories disclosed two other features. First, many i-FSSs correspond with Clarke's nucleus's shorter thoracic rostral extent, i.e., a hypotrophic state. Second, the low-tide and high-tide axons share a common pathway in the DC. The brown tint darkening reflects the gradual ripening of the neuropil. (b) At the downstream M_0 , fewer i-FSSs (marked: *) might coincide with the duly ripening of Clarke's nucleus, extending halfway up the thoracic spinal cord.

The features of the primordial configurations elicited variable access to the neuropil (see Figures 14 and 15). Figure 18a illustrates the DC-WM colls in the upper thoracic spinal cord without clear penetration or just the neuropil's fringe, as shown in the p3, p7, and p9 neonates and the p40 young adult. The dissociation indicated that the afferent system and the neuropil developed independently. The dissociation explained the label decrease in the proper colls, visualizing less of Clarke's nucleus. Enhancement of the label, in contrast, was also found in the cases of p7 and p9. At the lumbar level, the accessible neuropil showed a paradoxical enhanced label, while the dystopic multilevel colls in the upper thoracic spinal cord might have suggested impervious neuropil. The discrepancies in label enhancement might have a relationship with the dissociation caused after a Tx (see Section 4.2.4).

The variable impact on Clarke's nucleus development either due to an absolute or a transient hypoxia effect, enabling a stepwise ripening of the neuropil.

On the one hand, dissociation might have lowered the label intensity of inaccessible neuropil. On the other, signs of dissociation coincided with label enhancement at lumbar spinal cord levels. Extreme label enhancement showcased a second p7 neonate with an E17/E18 inadvertently oversized, i.e., complete transection at the lumbo–thoracic junction (see Figure 19a,b). Its p2 left sciatic nerve transection had aggravated the features on top

of the incidental total Tx. The isolated caudal spinal cord stump exhibited extreme enhancement from dorsal and ventral root tracing. This feature illustrates the preconditioning impact of epigenetic mechanisms, which might be appropriate to disclose through pathway analysis [24,25]. Figure 19c–f exhibit enhancement configurations at spinal levels, with comparable states of neuropil’s dissociation after Tx. The colls, indicated by a tandem asterisk, showed label enhancement in the DH down to the intermediate gray. This feature remained visible throughout the life of the caged rats, like the infinite label enhancement in the p700 case (see Figure 19f). The peripheral nerve transection might have boosted the intrinsic regenerative plan separately, shown for the first time in 1984 [26]. After that, peripheral nerve transection became a well-known indication of the creation of a preconditioning lesion.

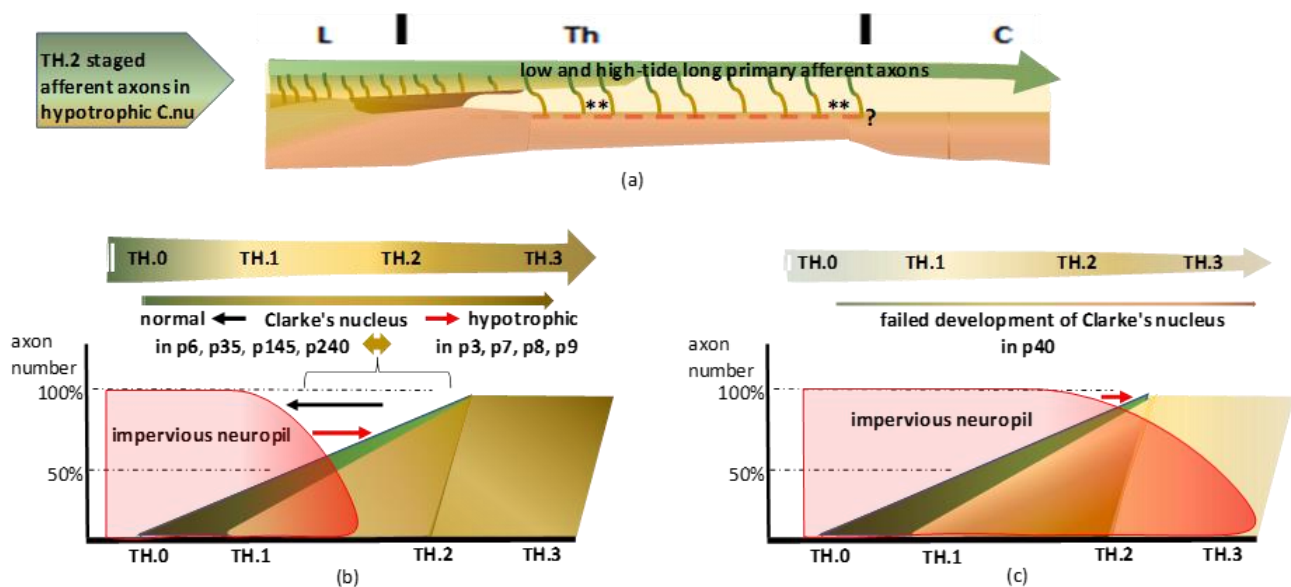


Figure 18. (a) The primordial state revealed a common course of high- and low-tide axons yielding numerous DC-WM colls (marked: **) in the upper thoracic spinal cord. After recovery from fetal hypoxia during the microsurgical procedure, the afferent axons might have started or continued pioneering the DC. The interruption might have retarded the neuropil’s ripening, shortening the accessibility period. The hypotrophic Clarke’s nucleus, due to the linked high–low-tide wave axon shift, yielded the upstream DC-WM harboring target-bound long colls. The long colls are shown in Figures 5c–e, 7c,d, 9c–f, 13c,d, 14c–f, 15c–f and 16d,f. The red-colored interrupted line indicates the impact of impervious neuropil, yielding similar signs of the primordial state in Figures 5, 7, 9–12 and 14–16. Concurrently, DC-WM long colls were present at dystopic upper thoracic levels. Their functionality is questioned (marked: ?). (b) The dissociation of the in neuropil embedded Clarke’s nucleus yielded a primordial state. Variable hyposaturation might have determined Clarke’s nucleus hypotrophy, reflecting the developmental conditions of the long primary afferent system. The listed eight cases are ordered from normal maturity to the hypotrophic state. The seemingly retarded neuropil ripening paralleled the restricted access of low-tide axons and illustrated the primordial state of Clarke’s nucleus. The hypotrophic Clarke’s nucleus is visible in the adult cases p35 and p240. (c) Severe retardation prevented the long primary afferent axons from penetrating the neuropil. Almost blank neuropil confirms a total absence of Clarke’s nucleus, shown in the p40 case. The uninterrupted red line in Figure 15a indicates that the inaccessibility might be a lasting feature. Considering the reverse of retardation, accelerated afferent axon development might present with similar features (see Section 4.2.4).

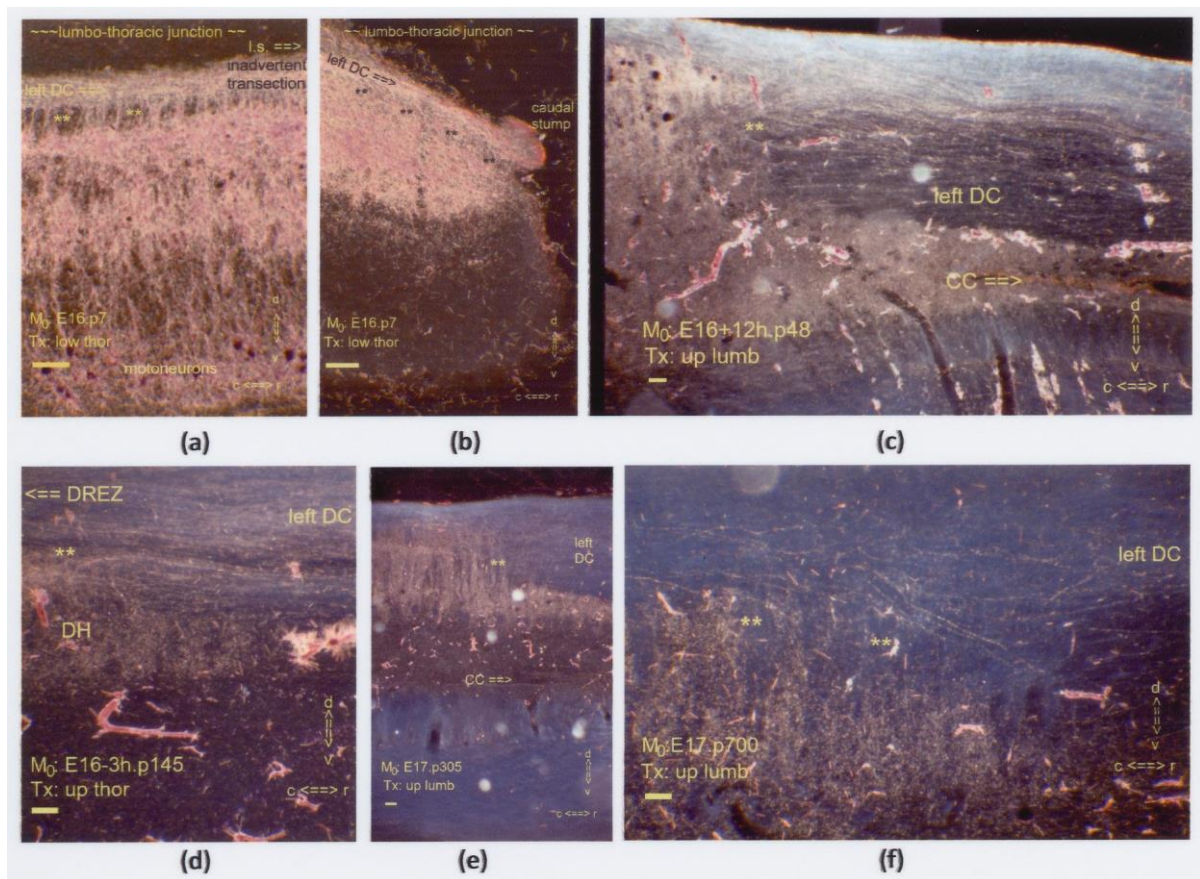


Figure 19. (a–f) Sagittal sections display boosted label in the DH’s central gray. These lumbar segments depict the levels just rostrally to the DREZ in five cases, which survived from one week to almost two years. (a,b) The p7 neonate exhibits the impact of an inadvertently oversized Tx at a low thoracic level with an additional lesion, i.e., a p2 transection of the left sciatic nerve. The label was present excessively throughout the central gray, delivered by anterograde and retrograde transport of DRG and motoneurons. The HRP was applied to the central stump of the left sciatic nerve and traced via the L4–L6 dorsal and ventral roots. This spinal cord’s caudal stump showcased label enhancement after preconditioning with a spinal cord and sciatic nerve transection. (c–f) The Tx sites were located at a few segments rostrally, except for the thoracic level in Figure (d). The enhanced label from colls (marked: **) remained a noticeable feature for almost two years in the caudal DH down to the intermediate gray. All scale bars: 100 μ m.

4. Discussion

The Blueprint’s Basics

The kaleidoscopic features of the axon tangled configurations show a plausible blueprint of the assembly line showcased by the ordered sets of stills. Key to the concept is a chain of hypothetical transition hubs (THs) stationed on the assembly line. The long primary afferent axon development narrative is told with the speculative spring and neap tides described by the corresponding Tx-rendered a-FS and i-FSSs. These tracing features showed that the cut axons recuperated after the Tx. We concluded that stepping down the cascade into the next stage of the DRG neuron’s intrinsic developmental plan was shown to be blocked. These transition blockades refer to THs disregarding their possible complex nature. The amount of time the stops might take and the involvement of a network of unknown interdependent transcription factors are taken for granted. Whether all of the pioneering primary afferent axons follow the same rules targeting either gracile or Clarke’s nuclei might be questioned. The bundled axon feature of the rostral Tx’s causing the a-FS

might differ phenotypically from the caudal Tx's causing the multilevel i-FSs. The perceived difference enables the distinction between the high- and low-tide axons.

Next to this direct impact on cut axons, the paradigm affected the neuropil, creating features of inaccessibility. This superimposed effect resulted in temporospatial dissociation. While the gracile nucleus was accessible at spring tide, axons might face an immature Clarke's nucleus impervious to axons at neap tide. The numerous low-tide i-FSs, cut before penetrating Clarke's nucleus, might coincide with persistent pioneering axons in the common subpial pathway. The more i-FSs there were, the less TH.2-staged axons had labeled Clarke's nucleus, suggesting hypotrophy. Delayed ripening of the neuropil likely interfered with the proper temporospatial development of the embodied Clarke's nucleus. The next sections cover the above issues revealed by the paradigm.

4.1. The Assembly Line

4.1.1. The Long Primary Afferent System Assembly at Four Transition Hubs

The assembly line's graphic depicts the axon waves at high and low tides (see Figure 2). The Tx-rendered features of the transition hubs TH.1 to TH.3 enabled a blueprint's concept, Balkanizing the development process and disregarding the complexity of the intrinsic developmental program [19]. The stratification with three THs causing distinguishable features offered a blueprint in the simplest format. The results uncovered cytoarchitectural configurations of the long primary afferent system. The uncut high-tide pioneering TH.0-staged axons targeted the gracile nuclei under any circumstance. Next, the axons transitioned into the hypothetical TH.1 stage. This first step down the cascade at spring tide is the fast elongation stop phenomenon (f-ES). Then, a noticeable progress awaited the formation of TH.2-staged colls visible in the gracile nucleus. By inference, a lapse in time might have interspaced TH.1 and TH.2. This period is called the slow elongation switch phenomenon (s-ES). Next, the colls penetrated gracile nuclei. Following a comparable intrinsic developmental plan, the colls penetrating Clarke's nucleus might have developed at neap tide. This cascade delineated a possible timeframe for the development of the two subdivisions. However, time lags and axon numbers were impossible to quantify. When appropriate, an approximation or a guess by inference came into place. The data revealed the myriads of multistage axons rendered at upstream axon development. An unidentified thrust forcing the long primary axons down the cascade might have restricted the CP, which may have taken more or less than 24 h. By inference, the data also indicated that the developmental tempo might have decreased gradually.

4.1.2. The Development Blockade in High and Low Tide Pioneering Axons Marks the Closure of the Critical Periods

TH.0-staged fibers started pioneering first, creating a high-tide wave. Regarding a rostrocaudal gradient, L4 axons might grow ahead of L5 and L6 axons until they elongate, forming multistage axons originating from the adjacent lumbar levels. Featuring multistage axons, they might reflect a fast elongation tempo during the upstream critical period (see Figure 3). Whether the a-FS mimicking the hypothetical f-ES phenomenon at the medulla might demand instant feedback for the TH.1 transition, like in the TH.0 axons, is questionable. After the Tx caused TH.1-staged axon terminations abutting the lesion site, the a-FS implicated cut axon repair. These TH.1 transitions might differ phenotypically from the TH.0-staged axons transitioning instantly at the medulla. The interrupted development and recovery might have taken long enough to signal and alter the proteomic signatures of the neurons, which closed their CPs. The tracing up to the lesion site confirmed antegrade label transport in viable neurons despite the blockade of further development down the cascade. At low tide, the i-FSs might have resulted from a similar but not identical mechanism, as the TH.1-staged axons recovered at shorter ranges [19]. Those permanent features illustrated the failure to transition further down the cascade. An alteration of the proteomic signatures might have abolished the intrinsic plan. The impact at low tide might involve the neuropil's embedded anlage when a caudal Tx rendered the so-called primordial state. The minor

labeling of the caudal Clarke's nucleus suggested a hypotrophic state at a dystopic location halfway down the DH.

The temporospatial separation between the a-FS and the ensuing s-ES might indicate a time lag, which might increase after Txs. A Tx at a rostral spinal cord level caused the neonatal a-FS of bundled high-tide axons while elongating, i.e., before they had transitioned into TH.1. The impact on low-tide axons featured the multilevel i-FSs at caudal spinal levels. Those features discriminated the lesioned fibers from TH.0-staged fibers, accomplishing the developmental cascade. Regarding the "spared axon conundrum," the a-FS and i-FS documented an unquestionable repair of the cut axon. They featured characteristics distinguishing them from the parent TH.0-staged axons [27].

4.1.3. Collaterals and Fiber Resorting: Development Impairment

TH.2-staged colls penetrating the gracile and Clarke's nucleus might differ phenotypically. The penetration of colls, commencing simultaneously at the remote levels, is in question here. The central and peripheral branches of the pseudounipolar DRG neuron might be considered purposeful of equal lengths. The governing intrinsic developmental plan would favor concomitant transitions into the TH.2 and TH.3 stages. Then, the central and peripheral targets could harmonize during the in-sync fiber-resorting process [28,29]. After a functional waiting period, a modality-based organization might be plausible [11].

Hypoxia may alter proteomic profiles, so the paradigm effects the upstream temporospatial development [24,25]. From the TH.2 stage onward, the formation of collaterals seemed unrestrained. Downstream axons might have featured seemingly regular phenotypes after Txs disengaged the targets. The dystopic ones may have impaired the fiber resorting process and synaps formation, harming the functional circuitries within the complex spinal networks. In the E16-9h.p6 case, many colls had found targets at dystopic levels across the lesion site (see Figure 9d-f). This feature classified the M_0 downstream compared to the E16-3h.p145 case, which exhibited an age-morphed a-FS (see Figure 10e). Also, the many TH.1-staged i-FSs in the DC-WM pointed upstream (see Figure 10c,d).

In addition to these dynamic features, the one tiny CG-facing FS on the contra-lateral side indicated dynamics over the left-sided tiny CG-facing FS. The right-sided TH.3-staged axons had to cross the midline beyond the damaged midline septum. The more dynamic features generally pointed to an unidentified factor upstream at the cascade. This factor revealed a tendency to decrease, which might refer to the high- and low-tide concept.

The Txs further downstream, i.e., at or beyond CP's closure, caused features of TH.3-staged axons to aggregate into root-like configurations. Beyond the assembly line, Txs might have activated final downstream proteomic profiles. They caused features of decreased potentiality in neonatal or adult central axons. This capacity assigned to matured axons might have responded to central lesions by reactivating downstream profiles just a few little steps backward on the cascade [19].

4.2. The Paradigm's Hypoxia Affecting Development

4.2.1. Clarke's Nucleus: A Dichotomic Construct

An intrinsic developmental plan governs the unknown temporospatial process of the long primary afferent axons. The experimental configurations showed that the Tx-rendered features of the primary afferent axons might link directly to a multistage development from TH.0 to TH.3 along the individual assembly lines from within the CP. The interpretation of our data favored a blueprint of an upstream common trajectory for all of the long primary afferent axons. The reciprocity between the individual courses implied versatility, delineating the CP. This phenomenon of compliance might support a modality-based organization opposite to the predestined somatic map model [11,30].

The L5 ganglion generates hundreds of long primary afferent axons [24]. From the caudal lumbar levels, the long primary afferents wave to the medulla at spring tide and are located dorsally in the DC-WM. This feature is shown in the primordial state. Along with protracted ripening of the neuropil, the anlage of Clarke's nucleus appeared gradually,

favoring the neap tide concept. Up to 15% of high-tide axons of DRG neurons target the gracile nuclei [31]. The low-tide axons targeted the anlage of Clarke's nucleus and might have executed a comparable plan. At upstream M_0 s, the Tx's blocked further development of these axons and precluded coll formation. They caused numerous i-FSs in the DC-WM when the Tx's were located at low thoracic levels. These multilevel parasagittal axons down the DC and at subpial positions exhibited permanent unequal distances to the lesion site.

Considering the primordial states in the p3, p9, and p40 cases, the subpial and sagittal locations illustrated the common trajectory for all pioneering long primary afferent axons. Their long colls crossing the depth of the DC and from the caudal to the upper rostral levels of the thoracic spinal cord may refer to this state. Inaccessibility indicates unripe neuropil. Therefore, we concluded that the two systems might develop independently. Moreover, the multilevel dystopic colls, i.e., at the upper thoracic level, mark this phenomenon of dissociated development. It is unclear whether the dystopic targets might add to a functional rostral extension of Clarke's nucleus.

A mid-thoracic Tx in the p240 case showed numerous i-FSs coinciding with a barely labeled Clarke's nucleus (see Figure 11d). The Tx prevented the cut axons from stepping down the cascade. Less colls had penetrated Clarke's nucleus. In contrast, the p35 and p195 cases showed fewer i-FSs. Clarke's nucleus was labeled more extensively and interpreted tentatively as a less hypotrophic state. An arguable inverse relationship was found between an apparently high number of i-FSs and whether Clarke's nucleus looked hypotrophic at the proper upstream M_0 . Considering the plausible common trajectory, the caudal Tx's disrupted a regular distribution between low- and high-tide axons. At these upstream M_0 s, the subpial fiber bundle might have encompassed a variable mix of pioneering high- and low-tide axons beyond Clarke's nucleus. The data might reveal randomness in whether low-tide axons duly formed colls in the embedded anlage of Clarke's nucleus, which depended on the ripening of the neuropil. With the dystopic location halfway down the DH, Clarke's nucleus's hypotrophy might also depict a shortened thoracic extent.

Overall, the long primary afferent system exhibited a remarkable capacity to comply with fallible states of the neuropil's development. Those configurations disclosed a neuron-dependent flexible adaptation capacity during the upstream state of pioneering axons, referred to as the critical period (CP). The temporospatial dissociation documented curtailed the assemblage of Clarke's nucleus. The data offered insights which may help to overcome the current ambivalent artwork on the system's cytoarchitecture [32]. Nonetheless, the issue of fiber branching in dorsal rootlets explaining discrepancies between neuron cell and axon counts remains unsolved [33]. It is imaginable, though, that accidentally and inadvertently backward-turned caudal branches in the bifurcation zone might account for inconsistent findings of dorsal root axons outnumbering the DRG neurons [34].

4.2.2. The Paradigm's Impact on the Ripening of the Neuropil

The upstream Tx's causing the a-FS and i-FSs illustrated the abolished transition beyond the TH.1 stage. The a-FS harbored high-tide long primary afferents abutting the lesion site. The multilevel i-FSs, distanced from the lesion site, were assigned to low-tide axons. All axons showed the direct impact of the Tx's.

The paradigm's hyposaturation effected the development of Clarke's nucleus indirectly. The neuropil's primordial state in the p40 case documented no sign of Clarke's nucleus relating to the neuropil's inaccessibility [10]. The boosted features of label enhancement in the p9 neonate exhibited the reverse regarding Clarke's nucleus at the caudal neuropil. In the first set of four neonates, Clarke's nuclei demonstrated various stages of development which might link with the variability of the neuropil's ripening states. The second set of adult rats showed temporospatial dissociation by combining the hypotrophic Clarke's nucleus with the direct effect of various i-FSs. Hypotrophy was manifested by the inferred low numbers of low-tide axons, which indulged the neuropil at the variable states of retarded ripening. This dependency determined an inverse relationship between hypotrophy and i-FSs, depicted graphically in Figures 17 and 18. First, we concluded that

the paradigm caused permanent characteristic features of blocked development in the long primary afferent axons cut at their critical periods. Secondly, the paradigm disclosed variable features of the neuropil's ripening, expressing the hypotrophy of Clarke's nucleus (see Figures 7 and 14). The numerous i-FSs in the adult cases might be linked to this hypotrophic state. So, the different states of the two subdivisions in the long primary afferent system development indicated that the neuropil ripened independently. The hypotrophic state might reflect a delay yielding the temporospatial dissociation.

At the upstream critical period, the dissociation reflected the paradigm's two-edged impact, causing an indirect superimposed effect from the plausibly protracted neuropil's ripening. Accessible neuropil was conditional to Clarke's nucleus's proper development. After Tx at the upstream M_0 s, axons might face poor accessibility depending on the neuropil's state. That indirect effect made confounding features difficult to ascertain when the neuropil showed seemingly mature features. They might have originated from possible variations of hypoxic conditions. A transient impact might explain the features of the p7 case (see Section 4.2.3).

4.2.3. The Dissociated Neuropil

At the upstream cascade, the Tx caused primordial features of the bilateral anlage of Clarke's nucleus located halfway down the dorsal horn. An increased distance from the central canal and a restricted rostral extent might distinguish the anlage from the normal location of the mature Clarke's nucleus. Stagnant growth of the neuropil might determine the dystopic location. Speculatively, the expanding dorsal horn's neuropil might push down the anlage towards the central location. The features of short and long colls crossing the DC straight and obliquely and targeting Clarke's nucleus might relate to such a passive force next to the spinal cord's longitudinal growth. The neuropil's circumferential expansion at upstream M_0 s might coincide with E15–E16's dorsal horn augmentation, tentatively associated with the anlage of Clarke's nucleus shifting down the DH. The data might justify a conclusion that the hypoxia exerted its effect upon the upstream neuropil at a state of neurogenesis. Depending on the unknown duration and depth of the hyposaturation, the different neurons suffering from hypoxia might have shown various effects. In this respect, the arterial vasculature is known for its penumbral supply of the spinal cord's thoracic–cervical junction [35]. The saturation jeopardized at this particular Tx level likely affected neuropil's ripening for the worse or the better when transient asphyctic conditions caused upstream fetal genomic signatures to restrict energy turnover, comparable to asphyctic preconditioning [24,36]. The dorsal horn's regular H-shape delineates after E17, i.e., beyond the long primary afferent system development [3]. Despite the dorsal halves being seemingly appropriate in the p3 and p8 neonates, and considering the neuropil's extent with the in-between labeled axons depicted mid-sagittally and deep down the DC, the neuropil might feature dissociation. The embedded anlage of Clarke's nucleus might have exhibited hypotrophy features correlating with the neuropil's temporospatial dissociation.

The p7 and the p9 neonates sharing different and similar features concerning the three subdivisions highlighted another issue. In the p7 neonate, the Tx at the level of Clarke's nucleus caused a loss of label in the left gracile nucleus, indicating the relative downstream M_0 . The further upstream M_0 in the p9 neonate yielded more TH.0-staged axons, which labeled gracile nuclei abundantly. At the upper thoracic levels, the dystopic colls in both cases indicated a primordial state. The neuropil at the intersegmental short subdivision targets showed extensive label in Rexed layers V–VII in the DH (see Figure 16c). The paradigm's induced hypoxia might have affected their neuropil briefly. It begs whether transient hypoxia goes with alleviated effects. These two cases might illustrate that the very upstream development, which is seemingly normal, exhibits overhauled features that mask the neuropil's dissociation. The possible variability of hyposaturation may determine the various features. Figure 18b,c depict the neuropil's dissociation graphically. The developmental dissociation related to the variable impact of hyposaturation might

affect tissue development stepwise. Examples of disruptive growth differing at remote levels in the spinal cord are presented in [37].

An artist's impression graphically depicting the long primary afferent system's development follows the steepest curve, as shown in Figure 2a. Tritiated thymidine studies in healthy E13–E16 fetal rats are in keeping with such an acute angle [38]. Long-distance tracing requires experiments on the living, as death might offer questionable results [3]. In epigenetic and proteomic mapping, current profiling tools might affect genuine profiles when processing dead tissue [39]. Conclusions based on unvalidated upstream tissue profiling results may lead us astray. Our results underline the rapid and enduring effect of transient hyposaturation. Rodent Hypoxia/Ischemia (H/I) models replicating the clinical symptoms of H/I in neonatal humans are used to investigate H/I-induced brain damage and develop therapeutic strategies [40]. Our paradigm may offer a tool suitable for exploring this research domain.

This paradigm may provide a unique microsurgical dissection tool. Its purpose is to peel off, layer by layer. The discovery of the primary afferent system's development succeeded by turning over the cards one by one, allowing us to look at them face up. An upcoming paper describes the impact of the paradigm at further upstream M_0 s and addresses the effects of TxS on the regeneration of high-tide TH.0-staged axons.

4.2.4. Dissociation Overhauled due to Variability of Transient Hypoxia

Our observations prompted speculation and suggested plausible mechanisms mentioned below. The central nervous system uses apoptotic cell death to level developmental neuron excess [41]. The excess neuropil of the p8 neonate was straightforward and attributable to fallible apoptosis. The whole-genome transcriptional changes, including epigenetic mechanisms, are assessed for total hypoxia in the rat uterine horn via arterial clamping for half an hour [25,42]. We may suggest that the variability of our results might have a relationship with various but unknown hypoxic conditions at stake. In the p8 neonate, the dorsal hump might relate to such an intercurrent alteration. This phenomenon, due to the neuropil's ripening which might have retarded beyond the CP of the long primary afferent axons, indicates that the two systems can develop independently. The cases at the primordial state exemplified a possible shift, illustrating unripe neuropil at or beyond the CP's presumptive closure of the primary afferent system. The p40 case demonstrated closure of the CP by TH.2-staged axon penetration in the gracile nucleus. Considering the thoracic–cervical junction, known for its penumbral vasculature, rostral thoracic levels are prone to hyposaturation [35]. Might this condition be at stake at the p8 rostral spinal level? The neuropil's excess was tentatively linked to spinal hyposaturation [41,43]. The neuropil's delayed ripening and the blockade of the DRG neuron's upstream development might illustrate this two-edged impact of the paradigm's transient hypoxia. TxS caused configurations of axons featuring a combination of cut axons with the neuropil's dissociated development. After the accomplished surgical procedure, it begs whether recovery from hypoxia and normal saturation might overhaul the dissociation and reconstitute normal development. The p7 and p9 neonates might offer examples exhibiting seemingly normal features of both systems.

The Long Primary Afferent Axons

Considering the dynamic features, the primordial state of the long primary afferents might have mitigated or obscured apoptosis. The upstream a-FS and the numerous i-FSs might contradict apoptosis. Indeed, the TxS might nullify an apoptotic mechanism when axonal anterograde transport is at its vertex [44]. The Tx-rendered a-FS and i-FSs reflected the dynamic capability of developing neurons, which also expressed versatility when considering the shift between low- and high-tide axons in the rostral DC. The neuropil's temporospatial dissociation-related reciprocity between low- and high-tide axons in the DC might balance axon reduction. The low-tide TH.1-staged axon terminations in the DC deprived of proper targets may raise the question of whether they survived anyway. Degeneration reduces the number of viable axons [45].

However, the numerous i-FSs in adult cases refuted an apoptotic mechanism at this upstream state. Further upstream, the DC-WM colls add another feature contradicting torpid apoptosis in aimless axons. In contrast, might axon excess be a plausible feature at the upstream state? The abundant label in the neuropil of the p7 (Figure 5c) and p9 (Figure 16c) neonates might point that way. The dystopic colls highlighted the primordial state, which might have lasted temporarily. When overhauled, further ripening of the neuropil might have yielded the high-tide axons developing normally down the cascade. Meanwhile, the low-tide axons might have persisted due to a simultaneous shift. Questionably, these axons might have contributed to the labeled gracile nuclei (see Figure 16g). There may have been an opportunity to level axon excess at the upstream cascade. Like in the primordial neuropil, apoptosis might have exerted its effect improperly in this more upstream state if present. Despite the upstream Tx also cutting low-tide axons, the features of the p7 neonate might indicate that a mix of all long primary afferent axons had contributed to the labeling of gracile nuclei. Moreover, the defectuous labeled left gracile nucleus pointed at an M_0 fallen downstream compared to the p9 neonate.

Retardation versus Acceleration in High- and Low-Tide Axons

Normal DRG neurons show a marked increase in cell diameter at E15 [46]. This phenomenon might link to the upstream axon elongation time window, delineating the critical period. Axon branching, the splitting at the axon tip, starts with the branching shortly from the DRG neuron, characterizing the pseudounipolar feature. The axon divides again at the DREZ bifurcation zone, and the terminal growth cone creates the final colls at the target level. The data revealed that the central axons could build terminal colls at various rostral levels in the DC-WM. The intrinsic developmental plan offered no apparent strategy which rigidly governed the axon's tip's whereabouts or the TH.2 transition schedule. On the contrary, the dystopic-level features implied that their CP's are wandering. Those dystopic colls indicated that the growth of the long primary afferent axons might have been retarded. Retardation might classify these colls as likely to originate from high-tide axons. Notably, low-tide axons might need consideration when transient asphyctic conditions restrict energy turnover. The paradoxical effect might be an acceleration of elongation. Accelerated growths of the long primary afferent axons might yield a similar effect of temporospatial dissociation comparable to delayed ripening of the neuropil (Figure 18c). So, the closure of the CP of the neuropil and the long primary afferent system is manipulable. A preset link enables proper development of both systems with an in-between time lapse. The paradigm's usage narrows or widens the gap between the CPs. By inference, the data indicate that such a natural order might even reverse. If acceleration occurs, the flowcharts A and B should switch positions in Figure 2a.

Sustained Features of the Primordial Neuropil

Considering the inferred natural decline of dynamic capabilities, the loss of dynamics might parallel the development progress. DRG neurons might suffer downstream from a residual drive to elongate down the developmental cascade, affecting the axons of the intermediate and short subdivision neurons the most. Near the closure of the CP, DRG neurons might abolish further initiation of pioneering axons, limiting the total number of long primary axons at the medulla. This mechanism also might limit the chance of axons encountering an inaccessible neuropil at a downstream M_0 .

Enhanced labeling in the caudal central gray might link to some primordial states of the neuropil but not in combination with sustained features of fallible apoptosis. Comparable features were still present in the last five cases (Figure 19a–f). Adding to this notion, the transected spinal cord of the p7 neonate demonstrated abundant CG labeling to which axons in all three subdivisions might have contributed (Figure 19a,b).

5. Conclusions

The feature myriads demonstrated that developmental interference disturbed the interaction between the long primary afferent system and the neuropil. The effects on the cut elongating long primary TH.0-staged axons were straightforward, i.e., a development

block. The unripe neuropil, impervious for colls to form Clarke's nucleus or penetrate the CG, demonstrated a temporospatial dissociation. This two-edged effect of the paradigm is due to hypoxia. The TxS caused seemingly random effects which might relate to undetermined variable degrees of hyposaturation. The depth and duration of hypoxia have been acknowledged as relevant parameters in developmental gene expression experiments [47]. In line with these recent findings, our paradigm may provide a feasible tool to elucidate potential regulators in the physiological pathways of the developing fetus via experimental variations of those established parameters. Above all, the developmental state of the neuron mattered as it might have determined great susceptibility to hypoxia in our study.

Translational Impact and Future Experimentation

The dissociated neuropil became manifest in the primordial state when the CP of the long primary afferent axons preceded the delayed ripening of the neuropil. Likewise, accelerated development of the long primary afferent axons might affect the neuropil, creating similar features of temporospatial dissociation. Absent parameters concerning fetal hyposaturation variations precluded the unsolved topics from being revealed in this study. Assessing those parameters on the length and depth of uterine hypoxia may elicit how and to what extent the TxS affected the neuropil's development [24,25]. Then, fetal sham operations may yield results that enable the filtering of the Tx-rendered features of the cut long primary afferent axons.

Regarding the upstream M_0 cases, KO studies in mice demonstrate a disruptive impact on the peripheral branches [48]. The phenomena above highlighted the paradigm's potential of *in vivo* genome engineering affecting the central branches. Above all, the potentially common trajectory of all pioneering axons revealed versatility that uncovered another characteristic of axon guidance adaptation [49]. The paradigm highlighted visible hypoxia-related effects during gestation, *i.e.*, before birth [40]. Regarding the primordial state, the inaccessible and blank neuropil might coincide with the development of the peripheral branch into the body's skin. Dissociation-based discrepancies between the systems might explain elusive clinical conditions, *e.g.*, painless channelopathy or congenital insensitivity to pain [50,51].

This paradigm showcased the capability of rendering an infinite phenotype from a finite transition hub, which might alter the chromatin landscape of transcriptomes [25]. This property may enable experimentation targeting molecular mechanisms to decipher a proper downstream natural order via pathway analysis [25,52]. Moreover, the paradigm may offer an efficient alternative gateway for exploring the reverse of converting mechanisms into less differentiated cells like iPS cells [53]. Research into hypoxia in tissue may benefit from identifying hypoxia markers and transcriptional kinetics' architectural complexity [54,55].

Future experimentation may settle the issues about the missing hypoxia parameters. The TxS at upstream developmental states exerted a two-edged impact. The long primary afferent axons demonstrated the direct effects. The interference at variable states of the neuropil's ripening exhibited the indirect effect of the paradigm's TxS at low tide's development of the embedded Clarke's nucleus. The paradigm highlighted the dissociation of development between the two systems. Hopefully, this paper may encourage further research, having blazed the trail.

Author Contributions: Conceptualization, F.C.d.B.; methodology, F.C.d.B.; analysis, F.C.d.B.; investigation, F.C.d.B.; writing—original draft preparation, F.C.d.B.; writing—review and editing, F.C.d.B. and H.W.S.; visualization, F.C.d.B.; supervision, H.W.S. All authors have read and agreed to the published version of the manuscript.

Funding: This research received no external funding.

Institutional Review Board Statement: Ethical review and approval were waived for this study due to the retrograde nature of the research which pre-dated the European legislation on animal welfare and institutional ethic board approval.

Informed Consent Statement: Not applicable.

Data Availability Statement: The data presented in this study are available on request from the corresponding author. The data will be publicly available in due time.

Conflicts of Interest: The authors declare no conflict of interest.

References

1. Wolpaw, J.R. The negotiated equilibrium model of spinal cord function. *J. Physiol.* **2018**, *596*, 3469–3491. [[CrossRef](#)]
2. Willis, W.D.; Coggeshall, R.E. *Sensory Mechanisms of the Spinal Cord*, 3rd ed.; Kluwer Academic/Plenum Publishers: New York, NY, USA, 2004; Volume 2, pp. 597–664.
3. Mirnics, K.; Koerber, H.R. Prenatal development of rat primary afferent fibers: II. Central projections. *J. Comp. Neurol.* **1995**, *355*, 601–614. [[CrossRef](#)] [[PubMed](#)]
4. Mirnics, K.; Koerber, H.R. Prenatal development of rat primary afferent fibers: I. Peripheral projection. *J. Comp. Neurol.* **1995**, *355*, 589–600. [[CrossRef](#)] [[PubMed](#)]
5. Mirnics, K.; Koerber, H.R. Properties of individual embryonic primary afferents and their spinal projections in the rat. *J. Neurophysiol.* **1997**, *78*, 1590–1600. [[CrossRef](#)] [[PubMed](#)]
6. Kitao, Y.; Robertson, B.; Kudo, M.; Grant, G. Neurogenesis of Subpopulations of rat lumbar dorsal root ganglion neurons including neurons projecting to the dorsal column nuclei. *J. Comp. Neurol.* **1996**, *371*, 249–257. [[CrossRef](#)]
7. Redmond, L.; Xie, H.; Ziskind-Conhaim, L.; Hockfield, S. Cues intrinsic to the spinal cord determine the pattern and timing of primary afferent growth. *Dev. Biol.* **1997**, *182*, 205–218. [[CrossRef](#)] [[PubMed](#)]
8. Watanabe, K.; Tamamaki, N.; Furuta, T.; Ackerman, S.L.; Ikenaka, K.; Ono, K. Dorsally derived netrin 1 provides an inhibitory cue and elaborates the “waiting period” for primary sensory axons in the developing spinal cord. *Development* **2006**, *133*, 1379–1387. [[CrossRef](#)]
9. Lallemand, F.; Ernfor, P. Molecular interactions underlying the specification of sensory neurons. *Trends Neurosci.* **2012**, *35*, 373–381. [[CrossRef](#)]
10. Chédotal, A. Roles of axon guidance molecules in neuronal wiring in the developing spinal cord. *Nat. Rev. Neurosci.* **2019**, *20*, 380–396. [[CrossRef](#)]
11. Niu, J.; Ding, L.; Li, J.J.; Kim, H.; Liu, J.; Li, H.; Moberly, A.; Badea, T.C.; Duncan, I.D.; Son, Y.J.; et al. Modality-based organization of ascending somatosensory axons in the direct dorsal column pathway. *J. Neurosci.* **2013**, *33*, 17691–17709. [[CrossRef](#)]
12. De Beer, F.C.; Thomeer, R.T.W.M.; Lakke, E.; De Vries, J.; Voogd, J. Spinal cord transections in fetal rats. Open intrauterine surgery with low mortality. *Brain Res.* **1988**, *454*, 397–399. [[CrossRef](#)]
13. De Beer, F.C.; Thomeer, R.T.W.M.; Lakke, E.; De Vries, J.; Voogd, J. Open Fetal spinal cord surgery in rats with low mortality achieved by prevention of oligohydramnios. *J. Neurosci. Meth.* **1992**, *42*, 11–17. [[CrossRef](#)] [[PubMed](#)]
14. De Beer, F.C. Dorsal myelotomy in E15–E16 fetal rat: A promising paradigm in regeneration research, with serendipitous transcriptomic effects on development of the primary afferent system. *J. Neurosci. Meth.* **2022**, *366*, 109402. [[CrossRef](#)] [[PubMed](#)]
15. Hilton, B.J.; Blanquie, O.; Tedeschi, A.; Bradke, F. High-resolution 3D imaging and analysis of axon regeneration in unsectioned spinal cord with or without tissue clearing. *Nat. Protoc.* **2019**, *14*, 1235–1260. [[CrossRef](#)]
16. Mesulam, M.-M.; Brushart, T.M. Transganglionic and anterograde transport of horseradish peroxidase across dorsal root ganglia: A tetramethylbenzidine method for tracing central sensory connections of muscles and peripheral nerves. *Neuroscience* **1979**, *4*, 1107–1117. [[CrossRef](#)] [[PubMed](#)]
17. Lanciego, J.L.; Wouterlood, F.G. Neuroanatomical tract-tracing techniques that did go viral. *Brain Struct. Funct.* **2020**, *225*, 1193–1224. [[CrossRef](#)] [[PubMed](#)]
18. Goodman, C.S.; Shatz, C.J. Developmental mechanisms that generate precise patterns of neuronal connectivity. *Cell* **1993**, *72* (Suppl. S10), 77–98. [[PubMed](#)]
19. Nieuwenhuis, B.; Eva, R. ARF6 and Rab11 as intrinsic regulators of axon regeneration. *Small GTPases* **2020**, *11*, 392–401. [[CrossRef](#)] [[PubMed](#)]
20. Chimelli, L.; Scaravilli, F. The development of the gracile nucleus in the rat: The time of ingrowth of ascending primary sensory fibers and effect of early deafferentation. *Neuroscience* **1987**, *22*, 661–670. [[CrossRef](#)]
21. Wessels, W.J.T.; Feirabend, H.K.P.; Marani, E. Development of projections of primary afferent fibers from the hindlimb to the gracile nucleus: A WGA-HRP study in the rat. *Dev. Brain Res.* **1991**, *63*, 265–279. [[CrossRef](#)]
22. Smith, C.L.; Hollyday, M. The development and postnatal organization of primary afferent projections to the rat thoracic spinal cord. *J. Comp. Neurol.* **1983**, *220*, 29–43. [[CrossRef](#)]
23. Molander, C.; Grant, G. Laminar distribution and somatotopic organization of primary afferent fibers from hindlimb nerves in the dorsal horn. A study by transganglionic transport of horseradish peroxidase in the rat. *Neuroscience* **1986**, *19*, 297–312. [[CrossRef](#)] [[PubMed](#)]
24. Cox-Limpens, K.E.M.; Vles, J.S.H.; Schlechter, J.; Zimmermann, L.J.I.; Strackx, E.; Gavilanes, A.W.D. Fetal brain genomic reprogramming following asphyctic preconditioning. *BMC Neurosci.* **2013**, *14*, 61. [[CrossRef](#)] [[PubMed](#)]
25. Cox-Limpens, K.E.M.; Vles, J.S.H.; Van den Hove, D.L.A.; Zimmermann, L.J.I.; Gavilanes, A.W.D. Fetal asphyctic preconditioning alters the transcriptional response to perinatal asphyxia. *BMC Neurosci.* **2014**, *15*, 67. [[CrossRef](#)]

26. Richardson, P.M.; Issa, V.M.K. Peripheral injury enhances central regeneration of primary sensory neurons. *Lett. Nat.* **1984**, *309*, 791–792. [[CrossRef](#)] [[PubMed](#)]
27. Steward, O.; Zheng, B.; Tessier-Lavigne, M. False Resurrections: Distinguishing Regenerated from Spared Axons in the Injured Central Nervous System. *J. Comp. Neurol.* **2003**, *459*, 1–8. [[CrossRef](#)] [[PubMed](#)]
28. Jackman, A.; Fitzgerald, M. Development of peripheral hindlimb and central spinal cord innervation by subpopulations of dorsal root ganglion cells in the embryonic rat. *J. Comp. Neurol.* **2000**, *418*, 281–298. [[CrossRef](#)]
29. Yamaguchi, Y.; Miura, M. Programmed cell death in neurodevelopment. *Dev. Cell* **2015**, *32*, 478–490. [[CrossRef](#)]
30. Rivero-Melián, C. Organization of hindlimb nerve projections to the rat spinal cord: A cholera toxin horseradish peroxidase study. *J. Comp. Neurol.* **1996**, *364*, 651–663. [[CrossRef](#)]
31. Giuffrida, R.; Rustioni, A. Dorsal root ganglion neurons projecting to the dorsal column nuclei of rats. *J. Comp. Neurol.* **1992**, *316*, 206–220. [[CrossRef](#)]
32. Attwell, C.L.; Zwieten, M.V.; Verhaagen, J.; Mason, M.R.J. The Dorsal Column Lesion Model of Spinal Cord Injury and Its Use in Deciphering the Neuron-Intrinsic Injury Response. *Dev. Biol.* **2018**, *78*, 926–951. [[CrossRef](#)] [[PubMed](#)]
33. Langford, L.A.; Coggeshall, R.E. Branching of sensory axons in the dorsal root and evidence for the absence of dorsal root efferent fibers. *J. Comp. Neurol.* **1979**, *184*, 193–204. [[CrossRef](#)] [[PubMed](#)]
34. Willis, W.D.; Coggeshall, R.E. *Sensory Mechanisms of the Spinal Cord*, 3rd ed.; Kluwer Academic/Plenum Publishers: New York, NY, USA, 2004; Volume 1, p. 98.
35. Tveten, L. Spinal cord vascularity. IV. The spinal cord arteries in the rat. *Acta Radiol. Diagn.* **1976**, *17*, 385–398. [[CrossRef](#)] [[PubMed](#)]
36. Wang, Y.; Wu, H.; Fontanet, P.; Codeluppi, S.; Akkuratova, N.; Petitpré, C.; Xue-Franzén, Y.; Niederreither, K.; Sharma, A.; Da Silva, F.; et al. A cell fitness selection model for neuronal survival during development. *Nat. Commun.* **2019**, *10*, 4137. [[CrossRef](#)] [[PubMed](#)]
37. Nallamshetty, S.; Chan, S.; Loscalzo, J. Hypoxia: A master regulator of microRNA biogenesis and activity. *Free Radic. Biol. Med.* **2013**, *64*, 20–30. [[CrossRef](#)] [[PubMed](#)]
38. Nandi, K.N.; Beal, J.A.; Knight, D.S. Neurogenic Period of Ascending Tract Neurons in the Upper Lumbar Spinal Cord of the Rat. *Exp. Neurol.* **1990**, *107*, 187–191. [[CrossRef](#)] [[PubMed](#)]
39. Shu, M.; Hong, D.; Lin, H.; Lu, F.; Huang, J.; Dai, J. Single-cell chromatin accessibility identifies enhancer networks driving gene expression during spinal cord development in mouse. *Dev. Cell* **2023**, *57*, 2761–2775.e6. [[CrossRef](#)]
40. Kletkiewicz, H.; Klimiuk, M.; Woźniak, A.; Mila-Kierzenkowska, C.; Dokładny, K.; Rogalska, J. How to improve the antioxidant defense in asphyxiated newborns—Lessons from animal models. *Antioxidants* **2020**, *9*, 898. [[CrossRef](#)] [[PubMed](#)]
41. Nguyen, T.T.M.; Gillet, G.; Popgeorgiev, N. Caspases in the Developing Central Nervous System: Apoptosis and Beyond. *Front. Cell Dev. Biol.* **2021**, *9*, 702404. [[CrossRef](#)]
42. Cox-Limpens, K.E.M.; Strackx, E.; Van den Hove, D.L.A.; Van Ekkendonk, J.R.A.; De Jong, M.; Zimmermann, L.J.I.; Steinbusch, H.W.M.; Vles, J.S.H.; Gavilanes, A.W.D. Fetal asphyctic preconditioning protects against perinatal asphyxia-induced apoptosis and astrogliosis in neonatal brain. *CNS Neurol. Disord. Drug Targets* **2015**, *14*, 33–40. [[CrossRef](#)]
43. Nornes, H.; Das, G. Temporal pattern of neurogenesis in spinal cord of rat. I. An autoradiographic study -time ad sites of origin and migration and settling of neuroblasts. *Brain Res.* **1974**, *73*, 121–138. [[CrossRef](#)]
44. Cheng, I.; Jin, L.; Rose, L.C.; Deppmann, C.D. Temporally restricted death and the role of p75NTR as a survival receptor in the developing sensory nervous system. *Dev. Neurobiol.* **2018**, *78*, 701–717. [[CrossRef](#)] [[PubMed](#)]
45. Coggeshall, R.E.; Pover, C.M.; Fitzgerald, M. Dorsal root ganglion cell death and surviving cell numbers in relation to the development of sensory innervation in the rat hindlimb. *Dev. Brain Res.* **1994**, *82*, 193–212. [[CrossRef](#)] [[PubMed](#)]
46. Lawson, S.; Caddy, K.; Biscoe, T. Development of rat dorsal root ganglion neurons Studies of cell birthdays and changes in mean cell diameter. *Cell Tiss. Res.* **1974**, *153*, 399–413. [[CrossRef](#)] [[PubMed](#)]
47. Lopez-Anguaita, N.; Gassaloglu, S.I.; Stötzel, M.; Bolondi, A.; Conkar, D.; Typou, M.; Buschow, R.; Veenvliet, J.V.; Bulut-Karslioglu, A. Hypoxia induces an early primitive streak signature, enhancing spontaneous elongation and lineage representation in gastruloids. *Development* **2022**, *149*, dev200679. [[CrossRef](#)] [[PubMed](#)]
48. Maor-Nof, M.; Romi, E.; Shalom, H.S.; Ulisse, V.; Raanan, C.; Nof, A.; Leshkowitz, D.; Lang, R.; Yaron, A. Axonal Degeneration Is Regulated by a Transcriptional Program that Coordinates Expression of Pro- and Anti-degenerative Factors. *Neuron* **2016**, *92*, 991–1006. [[CrossRef](#)] [[PubMed](#)]
49. Ducuing, H.; Gardette, T.; Pignata, A.; Tauszig-Delamasure, S.; Castellani, V. Commissural axon navigation in the spinal cord: A repertoire of repulsive forces is in command. *Semin. Cell Dev. Biol.* **2019**, *85*, 3–12. [[CrossRef](#)]
50. Waxman, S.G.; Dib-Hajj, S.D. The Two Sides of Na V 1.7: Painful and Painless Channelopathies. *Neuron* **2019**, *101*, 765–767. [[CrossRef](#)]
51. Spiteri, M.; Mifsud, M.; Azzopardi, T.; Giele, H. Population Study of Hand and Wrist Manifestations of Congenital Insensitivity to Pain. *Hand* **2022**, *17*, 155–161. [[CrossRef](#)]
52. Van Den Hurk, M.; Kenis, G.; Bardy, C.; Van Den Hove, D.L.; Gage, F.H.; Steinbusch, H.W.; Rutten, B.P. Transcriptional and epigenetic mechanisms of cellular reprogramming to induced pluripotency. *Epigenomics* **2016**, *8*, 1131–1149. [[CrossRef](#)]
53. Papp, B.; Plath, K. Reprogramming to pluripotency: Stepwise resetting of the epigenetic landscape. *Cell Res.* **2011**, *21*, 486–501. [[CrossRef](#)] [[PubMed](#)]

-
54. Beagan, J.A.; Pastuzyn, E.D.; Fernandez, L.R.; Guo, M.H.; Feng, K.; Titus, K.R.; Chandrashekar, H.; Shepherd, J.D.; Phillips-Cremins, J.E. Three-dimensional genome restructuring across timescales of activity-induced neuronal gene expression. *Nat. Neurosci.* **2020**, *23*, 707–717. [[CrossRef](#)] [[PubMed](#)]
 55. Fujita, Y.; Pather, S.R.; Ming, G.; Song, H. 3D spatial genome organization in the nervous system: From development and plasticity to disease. *Neuron* **2022**, *110*, 2902–2915. [[CrossRef](#)] [[PubMed](#)]

Disclaimer/Publisher’s Note: The statements, opinions and data contained in all publications are solely those of the individual author(s) and contributor(s) and not of MDPI and/or the editor(s). MDPI and/or the editor(s) disclaim responsibility for any injury to people or property resulting from any ideas, methods, instructions or products referred to in the content.